A thesis submitted for the degree of
Master of Science

Large Eddy Simulation of an Internal combustion engine incorporating a novel boundary layer modelling approach to evaluate piston-wall interactions

Yannick Durindel
Chair of Fluid Dynamics
University of Duisburg-Essen
30 January 2026

Primary Supervisor: M. Sc. Luiz Felipe Rico Cortez
University of Duisburg-Essen
Secondary Supervisor: Prof. Dr.-Ing Kempf
University of Duisburg-Essen

Abstract

Internal combustion engines remain a critical technology for transportation and power generation, with ongoing development focused on improving efficiency and reducing emissions. Accurate computational fluid dynamics (CFD) simulations are essential tools for understanding and optimizing in-cylinder flows and combustion. However, the wall-bounded turbulent flows in engines present significant modeling challenges due to their inherently non-equilibrium nature.

Wall-bounded flows near the piston, cylinder head, and liner surfaces form boundary layers that directly affect mixing and combustion efficiency. Unlike steady external flows where classical wall functions perform well, engine boundary layers experience rapid pressure changes, flow reversal, and unsteady forcing throughout the engine cycle. These non-equilibrium effects cause classical wall function assumptions—based on equilibrium boundary layer theory—to break down, potentially introducing significant errors in wall shear stress predictions.

This thesis develops and validates a novel wall treatment approach for Large Eddy Simulation (LES) of internal combustion engine flows. The enhanced viscosity wall treatment increases the effective molecular viscosity near walls to account for unresolved turbulent transport, mimicking the diffusive effect of near-wall eddies without requiring equilibrium assumptions. The approach is specifically designed for compatibility with immersed boundary methods, enabling efficient simulation of complex moving geometries such as the piston and valves.

The methodology is implemented in PsiPhi, an in-house CFD solver developed at the University of Duisburg-Essen for turbulent reacting flow simulations. PsiPhi employs structured Cartesian grids with immersed boundary methods for geometry representation, providing computational efficiency and natural handling of moving boundaries.

Validation is performed using turbulent channel flow at friction Reynolds number $Re_\tau = 395$. Direct Numerical Simulation (DNS) provides reference data for the mean velocity profile and wall shear stress. LES with the enhanced viscosity wall treatment demonstrates:

- Recovery of the correct velocity profile shape in both viscous and logarithmic layers
- Wall shear stress predictions within 5% of DNS values
- Significant computational savings compared to wall-resolved LES
- Robustness across a range of grid resolutions

Following validation, the enhanced viscosity wall treatment is applied to LES of the University of Duisburg-Essen optical engine under motored conditions. The optical engine provides experimental PIV data for comparison, enabling assessment of the simulation accuracy. The engine simulations capture:

- Development and breakdown of the tumble vortex during intake and compression
- Non-equilibrium boundary layer behavior under rapid pressure changes
- Spatial and temporal variation of wall shear stress across the piston surface

- Consistent wall treatment on all surfaces including the moving piston

The computational cost of engine LES with the enhanced viscosity wall treatment is reduced by approximately an order of magnitude compared to wall-resolved approaches, making multi-cycle simulations feasible with current high-performance computing resources.

Key contributions of this work include:

1. Development of an enhanced viscosity wall treatment that avoids equilibrium assumptions
2. Demonstration of compatibility with immersed boundary methods for moving geometries
3. Validation against DNS and analytical solutions in channel flow
4. Application to realistic engine geometry with comparison to PIV measurements
5. Practical demonstration of computational efficiency gains

The results demonstrate that the enhanced viscosity wall treatment provides a viable approach for practical engine simulations, capturing the essential physics of wall-bounded flows while maintaining computational tractability. The methodology contributes to the ongoing effort to develop predictive CFD tools for internal combustion engine design and optimization.

Acknowledgment

Contents

List of Tables

List of Figures

List of Code

List of Abbreviations

DNS	Direct Numerical Simulation
FVM	Finite Volume Method
LES	Large Eddy Simulation
RANS	Reynolds-Averaged Navier-Stokes
SGS	Subgrid-Scale

1. Introduction

Wall-bounded flows are inherently complex because they give rise to boundary layers. Near the wall, steep velocity gradients develop due to the no-slip condition. In internal combustion engines, these layers form along multiple surfaces, with the piston being particularly significant due to its large area, continuous motion, and strong influence on large-scale flow structures such as the tumble vortex.

1.1 Motivation

1.1.1 Boundary Layers in Internal Combustion Engines

Unlike steady external flows, engine flows are highly unsteady and dominated by pressure fluctuations and non-equilibrium effects. The in-cylinder flow undergoes rapid changes during the intake, compression, combustion, and exhaust strokes, creating a complex turbulent environment where classical boundary layer assumptions often fail.

The piston surface plays a critical role in engine flow dynamics:

- Large surface area exposed to combustion gases
- Continuous motion affecting the boundary layer development
- Strong influence on the tumble vortex and large-scale flow structures

Accurate prediction of wall shear stress at the piston surface is essential for:

- Understanding in-cylinder mixing and flow patterns
- Predicting boundary layer behavior during combustion
- Optimizing combustion chamber design

1.1.2 Limitations of Classical Wall Functions

Classical boundary-layer theory, developed mainly for steady conditions, describes how shear stress evolves with distance from the wall through three distinct regions: the viscous sublayer, the buffer layer, and the logarithmic region. Wall functions have been proposed to relate wall distance to shear stress across these zones, enabling coarse grid simulations.

However, the assumptions underlying these wall functions fail under the rapidly changing and confined conditions of internal combustion engines:

- Non-equilibrium effects due to rapid pressure changes
- Strong adverse pressure gradients during compression
- Flow reversal and boundary layer separation
- Complex geometry effects near valve seats and piston bowl

Inaccurate wall shear-stress estimation leads to errors in predicting boundary layer behavior and in-cylinder flow dynamics.

1.2 Challenges in Engine Simulation

1.2.1 Computational Cost

Because of the high velocities and turbulence in engines, fully resolving all flow structures through Direct Numerical Simulation (DNS) is impractical. The Reynolds numbers encountered in typical engine operation would require computational resources far beyond current capabilities.

Large Eddy Simulation (LES) offers a practical approach by resolving the large, energy-containing eddies while modeling the smaller scales. However, LES relies on Subgrid-Scale (SGS) models to represent the unresolved turbulence, and the accuracy of these models near walls remains a significant challenge.

1.2.2 Near-Wall Modeling Gap

A significant knowledge gap remains in developing SGS models that can accurately capture boundary-layer formation near the piston during the engine cycle. The standard approaches either:

- Require extremely fine grids near walls (wall-resolved LES), making simulations prohibitively expensive
- Use wall functions that fail under engine-relevant conditions (wall-modeled LES)

This motivates the development of novel wall treatment approaches that can handle the non-equilibrium conditions in engines while maintaining computational efficiency.

1.3 Objectives of This Work

This project aims to improve the physical understanding of near-wall processes in internal combustion engines and propose a novel modeling approach that accounts for boundary-layer effects. The key innovation is the introduction of a locally increased molecular viscosity near the walls, which are modeled using immersed boundaries.

The specific objectives are:

1. Generation of a CAD model of the University of Duisburg-Essen optical engine, with emphasis on accurate valve seat geometry
2. Generation of a numerical grid for the optical engine with 0.2 mm cell size
3. Development of a 1D model incorporating molecular viscosity manipulation near walls
4. Verification of the model using standard wall functions
5. LES of a simplified engine configuration including the 1D model
6. Grid sensitivity analysis to identify potential model improvements
7. LES of the full optical engine including the wall treatment model
8. Testing of different numerical frameworks: time integration and discretization schemes
9. Post-processing of simulation results with focus on piston-wall phenomena

1.4 Methodology

1.4.1 Enhanced Viscosity Approach

The proposed wall treatment introduces a locally increased molecular viscosity in the near-wall region to account for unresolved turbulent transport. Unlike traditional wall functions that prescribe velocity profiles, this approach modifies the effective viscosity to produce the correct wall shear stress on coarser grids.

The enhanced viscosity is applied within cells adjacent to the wall, where the immersed boundary method is used to represent the solid surfaces. This combination allows:

- Flexible handling of complex, moving geometries (piston motion)
- Smooth transition between near-wall and bulk flow regions
- Compatibility with existing LES subgrid-scale models

1.4.2 Immersed Boundary Method

The immersed boundary method represents solid surfaces that do not conform to the computational grid. This approach is particularly suited for engine simulations where:

- The piston moves through the domain during the simulation
- Complex valve and port geometries must be captured
- Grid generation for body-fitted meshes would be challenging

The wall treatment is integrated with the immersed boundary formulation to ensure consistent application of the enhanced viscosity near all solid surfaces.

1.4.3 1D Model Development

A one-dimensional model is developed to relate the enhanced viscosity to the local flow conditions and wall distance. This model:

- Captures the essential physics of the near-wall region
- Is computationally efficient for application in three-dimensional LES
- Can be verified against standard wall function predictions
- Is calibrated to produce correct wall shear stress behavior

1.4.4 Optical Engine Application

The University of Duisburg-Essen optical engine serves as the primary application case. Optical engines provide:

- Well-characterized geometry and operating conditions
- Experimental data for validation (when available)
- Representative engine flow features (tumble, swirl, squish)
- Realistic boundary layer development on the piston surface

1.5 Focus Areas

The post-processing and analysis focus on piston-wall phenomena:

1.5.1 Shear Stress Evolution

The wall shear stress distribution over the piston surface is analyzed throughout the engine cycle. Key aspects include:

- Temporal evolution during intake, compression, and expansion
- Spatial distribution across the piston crown
- Influence of the tumble vortex on local shear stress
- Comparison with standard wall function predictions

1.5.2 Boundary Layer Behavior

The boundary layer structure and behavior are examined, including:

- Boundary layer thickness evolution
- Assessment of boundary layer detachment and reattachment
- Non-equilibrium effects during rapid transients
- Interaction with large-scale flow structures

1.6 Thesis Outline

This thesis is organized as follows:

Chapter 2: State of the Art reviews the fundamental theory of turbulent flows and simulation methods. Conservation laws and the Navier-Stokes equations are presented, followed by the concepts of turbulence and the energy cascade. The three main simulation approaches—DNS, Reynolds-Averaged Navier-Stokes (RANS), and LES—are described, with particular attention to LES filtering and subgrid-scale models. Wall treatment methods, immersed boundary techniques, and engine flow characteristics are introduced.

Chapter 3: Numerical Methods describes the PsiPhi solver used in this work. The spatial and temporal discretization schemes are presented, along with the pressure-velocity coupling algorithm. The implementation of LES, immersed boundaries, and the enhanced viscosity wall treatment are detailed.

Chapter 4: CAD Model and Engine Geometry presents the development of the CAD model for the optical engine used in this study. The engine geometry, based on the AVL 5811 single-cylinder research engine at the University of Duisburg-Essen, is described along with the computational domain and mesh generation process.

Chapter 5: Channel Flow Validation presents the validation of the enhanced viscosity wall treatment using turbulent channel flow simulations. The channel flow at friction Reynolds number $Re_\tau = 395$ serves as the primary validation case, allowing direct comparison between DNS, LES, and analytical solutions.

Chapter 6: Engine Simulation presents the application of the enhanced viscosity wall treatment to Large Eddy Simulation of the optical engine. Building on the validation from channel flow, the wall model is tested under the challenging non-equilibrium conditions characteristic of internal combustion engine flows.

Chapter 7: Conclusion summarizes the findings of this work, discusses limitations, and suggests directions for future research.

2. State of the Art

This chapter presents the theoretical foundations required for understanding the numerical simulation of turbulent flows in internal combustion engines. Starting from the fundamental conservation laws, we derive the governing equations and introduce the concepts of turbulence modeling that form the basis of this work.

2.1 Conservation Laws

The behavior of fluid flows is governed by the fundamental conservation principles of mass, momentum, and energy. These laws, when expressed in differential form, yield the equations that describe the motion of fluids.

2.1.1 Conservation of Mass

The principle of mass conservation states that mass can neither be created nor destroyed. For a control volume, this yields the continuity equation:

$$\frac{\partial \rho}{\partial t} + \nabla \cdot (\rho \mathbf{u}) = 0 \tag{2.1}$$

where ρ is the fluid density and $\mathbf{u}$ is the velocity vector. For incompressible flows, where density variations are negligible, this simplifies to:

$$\nabla \cdot \mathbf{u} = 0 \tag{2.2}$$

2.1.2 Conservation of Momentum

Newton's second law applied to a fluid element yields the momentum equation. The rate of change of momentum equals the sum of all forces acting on the fluid:

$$\frac{\partial (\rho \mathbf{u})}{\partial t} + \nabla \cdot (\rho \mathbf{u} \otimes \mathbf{u}) = -\nabla p + \nabla \cdot \boldsymbol{\tau} + \rho \mathbf{g} \tag{2.3}$$

where p is the pressure, $\boldsymbol{\tau}$ is the viscous stress tensor, and $\mathbf{g}$ represents body forces such as gravity.

For a Newtonian fluid, the viscous stress tensor is related to the strain rate tensor by:

$$\boldsymbol{\tau} = \mu \left(\nabla \mathbf{u} + (\nabla \mathbf{u})^T - \frac{2}{3} (\nabla \cdot \mathbf{u}) \mathbf{I} \right) \tag{2.4}$$

where μ is the dynamic viscosity and $\mathbf{I}$ is the identity tensor.

Physical Interpretation of the Conservation Laws These conservation equations form the foundation of all fluid dynamics simulations, but their physical meaning deserves careful consideration. The continuity equation (Eq. 2.1) expresses a fundamental principle: fluid cannot simply appear or disappear. In an engine cylinder, this means that any gas entering through the intake valve must either remain in the cylinder or exit through the exhaust—there are no other options. For incompressible flows (Eq. 2.2), this constraint becomes even simpler: the velocity field must be divergence-free, meaning that fluid cannot accumulate or deplete at any point.

The momentum equation (Eq. 2.3) is essentially Newton's second law applied to a fluid. The left-hand side represents the rate of change of momentum, while the right-hand side accounts for all forces: pressure gradients that push fluid from high to low pressure regions, viscous stresses that resist deformation, and body forces like gravity. In engine flows, the pressure gradient term dominates during compression and expansion strokes, while viscous effects become critical near walls where the no-slip condition must be satisfied.

The stress tensor (Eq. 2.4) deserves special attention for wall-bounded flows. Near a solid surface, velocity gradients become large as the flow transitions from zero velocity at the wall to the bulk flow velocity. These gradients, when multiplied by viscosity, produce the wall shear stress that directly affects fuel-air mixing in engines. Understanding and accurately predicting this wall shear stress is central to the work presented in this thesis.

2.1.3 Conservation of Energy

The first law of thermodynamics, applied to a fluid element, gives the energy equation:

$$\frac{\partial(\rho E)}{\partial t} + \nabla \cdot ((\rho E + p)\mathbf{u}) = \nabla \cdot (\kappa \nabla T) + \nabla \cdot (\boldsymbol{\tau} \cdot \mathbf{u}) + \rho \mathbf{g} \cdot \mathbf{u} \tag{2.5}$$

where E is the total energy per unit mass, κ is the thermal conductivity, and T is the temperature. While the energy equation is important for combustion simulations, this thesis focuses on the momentum equations and boundary layer dynamics.

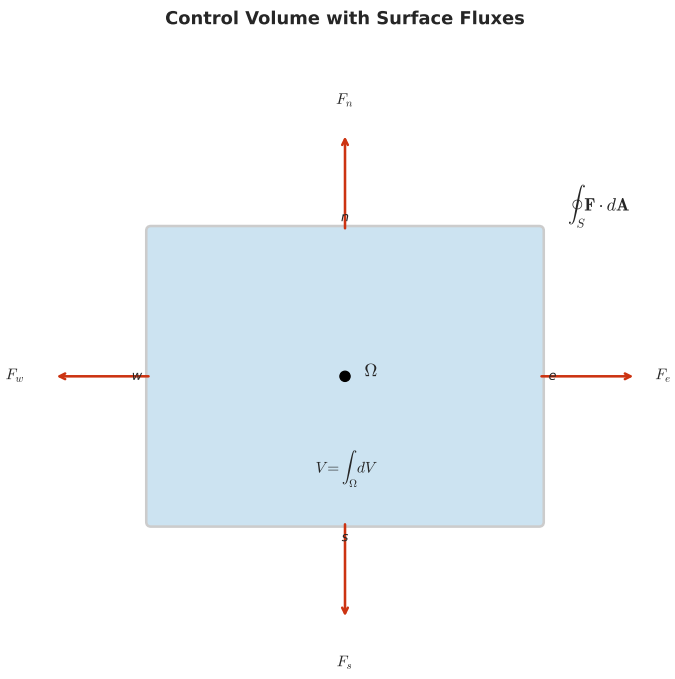

Figure 2.1: Control volume representation showing surface fluxes. The integral conservation laws are applied to such a finite volume, with fluxes crossing each face. This forms the basis of the finite volume discretization used in PsiPhi.

2.2 The Navier-Stokes Equations

Combining the conservation laws with the constitutive relations for a Newtonian fluid yields the Navier-Stokes equations. For an incompressible fluid with constant viscosity,

these take the form:

$$\nabla \cdot \mathbf{u} = 0 \tag{2.6}$$

$$\frac{\partial \mathbf{u}}{\partial t} + (\mathbf{u} \cdot \nabla)\mathbf{u} = -\frac{1}{\rho}\nabla p + \nu \nabla^2 \mathbf{u} + \mathbf{f} \tag{2.7}$$

where $\nu = \mu/\rho$ is the kinematic viscosity and $\mathbf{f}$ represents external body forces per unit mass.

The nonlinear convective term $(\mathbf{u} \cdot \nabla)\mathbf{u}$ is responsible for the complex behavior observed in fluid flows, including the phenomenon of turbulence.

2.2.1 Reynolds Number

The Reynolds number is a dimensionless quantity that characterizes the ratio of inertial forces to viscous forces:

$$Re = \frac{UL}{\nu} \tag{2.8}$$

where U is a characteristic velocity and L is a characteristic length scale. At low Reynolds numbers, viscous forces dominate and the flow remains laminar. As the Reynolds number increases beyond a critical value, the flow transitions to turbulence.

2.3 Turbulence

Turbulence is characterized by chaotic, three-dimensional, unsteady fluid motion with a wide range of length and time scales. Understanding turbulence is essential for accurate prediction of flow behavior in engineering applications.

2.3.1 Characteristics of Turbulent Flows

Turbulent flows exhibit several distinctive features:

- **Irregularity**: The flow variables fluctuate randomly in space and time
- **Three-dimensionality**: Even flows with two-dimensional mean properties have three-dimensional turbulent fluctuations
- **Diffusivity**: Enhanced mixing and transport of momentum, heat, and mass
- **Dissipation**: Kinetic energy is continuously converted to internal energy through viscous dissipation
- **Wide range of scales**: From the largest energy-containing eddies to the smallest dissipative scales

2.3.2 Reynolds Decomposition

To analyze turbulent flows, variables are decomposed into mean and fluctuating components. For any flow variable ϕ:

$$\phi = \bar{\phi} + \phi' \tag{2.9}$$

where $\bar{\phi}$ is the time-averaged (or ensemble-averaged) mean and ϕ' is the fluctuating component. By definition, $\overline{\phi'} = 0$.

Applying this decomposition to the velocity field:

$$u_i = \bar{u}_i + u_i' \tag{2.10}$$

2.3.3 Reynolds-Averaged Navier-Stokes Equations

Substituting the Reynolds decomposition into the Navier-Stokes equations and time-averaging yields the Reynolds-Averaged Navier-Stokes (RANS) equations:

$$\frac{\partial \bar{u}_i}{\partial t} + \bar{u}_j \frac{\partial \bar{u}_i}{\partial x_j} = -\frac{1}{\rho}\frac{\partial \bar{p}}{\partial x_i} + \nu \frac{\partial^2 \bar{u}_i}{\partial x_j \partial x_j} - \frac{\partial \overline{u_i' u_j'}}{\partial x_j} \tag{2.11}$$

The term $\overline{u_i' u_j'}$ represents the Reynolds stress tensor, which arises from the nonlinear convective term and requires modeling. This is known as the closure problem of turbulence.

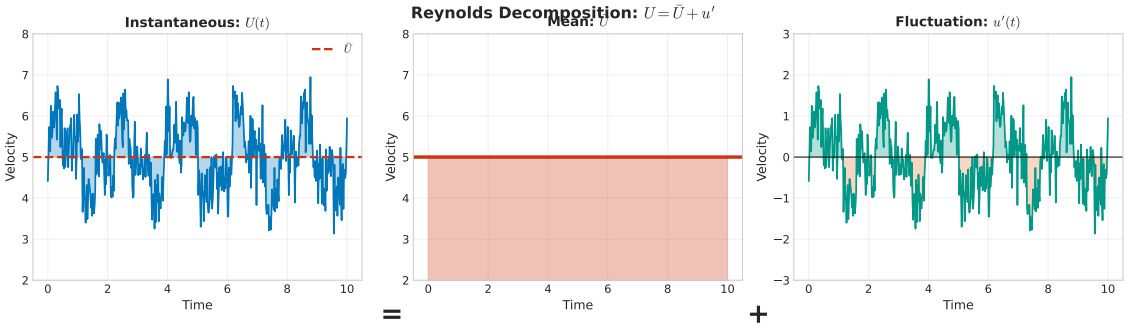

Figure 2.2: Reynolds decomposition of a turbulent velocity signal. The instantaneous velocity $U(t)$ is split into a time-averaged mean $\bar{U}$ and a fluctuating component $u'(t)$. The fluctuations are responsible for enhanced mixing and transport in turbulent flows, but they also introduce the closure problem that necessitates turbulence modeling.

Physical Meaning of Reynolds Stresses The Reynolds stress term $\overline{u_i' u_j'}$ deserves careful interpretation. Although it appears as a stress in the averaged equations, it actually represents turbulent momentum transport. Consider two fluid parcels passing a point at different instants: if a parcel moving faster than average ($u' > 0$) also tends to be moving away from the wall ($v' > 0$), then on average there is a net transport of high-momentum fluid away from regions of high momentum. This correlation between fluctuating velocities is the physical mechanism behind turbulent mixing—it is far more effective than molecular diffusion alone.

In engines, turbulent mixing is essential for preparing a homogeneous fuel-air mixture before ignition. The Reynolds stresses quantify this mixing intensity and must either be resolved directly (in DNS or LES) or modeled (in RANS) to predict engine performance accurately.

2.3.4 Energy Cascade

Richardson's concept of the energy cascade describes how energy is transferred from large to small scales in turbulent flows. Large eddies, containing most of the kinetic energy, are unstable and break down into smaller eddies. This process continues until the eddies become small enough that viscous forces dissipate their energy as heat.

Kolmogorov's theory provides scaling laws for the smallest scales of turbulence. The

Kolmogorov length scale η, time scale τ_η, and velocity scale u_η are:

$$\eta = \left(\frac{\nu^3}{\varepsilon}\right)^{1/4} \tag{2.12}$$

$$\tau_\eta = \left(\frac{\nu}{\varepsilon}\right)^{1/2} \tag{2.13}$$

$$u_\eta = (\nu\varepsilon)^{1/4} \tag{2.14}$$

where ε is the turbulent dissipation rate.

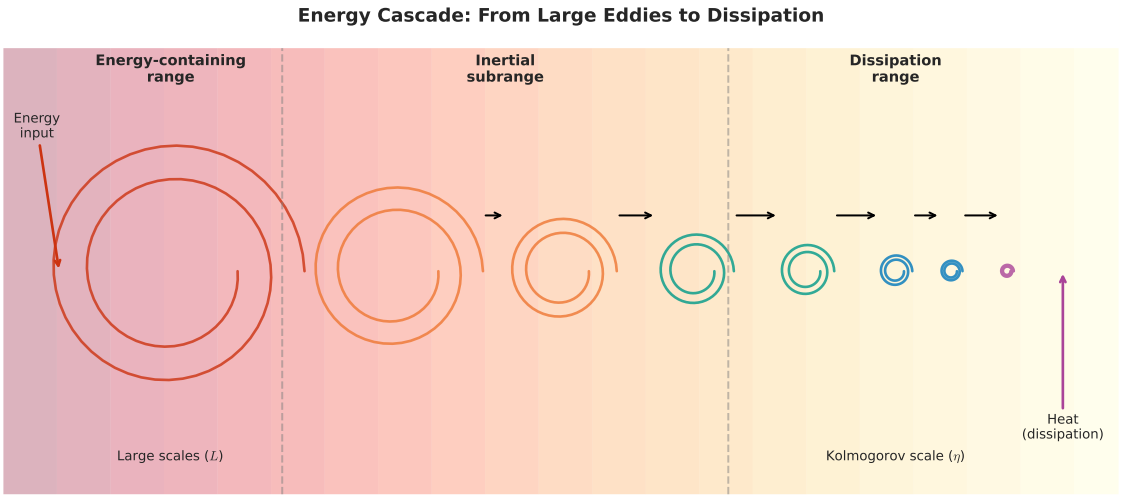

Figure 2.3: The energy cascade in turbulent flows. Energy enters at the largest scales through instabilities and mean flow gradients, then cascades through the inertial subrange where energy is transferred without significant dissipation. Finally, at the Kolmogorov scale η, viscous forces convert kinetic energy into heat. The ratio between the largest and smallest scales increases with Reynolds number, making high-Re flows computationally challenging.

Implications for Engine Simulations The energy cascade has profound implications for engine simulations. In a typical engine at operating conditions, the Reynolds number based on bore and piston speed can exceed 10^5, meaning the ratio between the largest eddies (comparable to the bore) and the smallest eddies (the Kolmogorov scale) can be several thousand. To resolve all these scales in a DNS would require a grid with billions of points and time steps small enough to capture the fastest fluctuations—a computational cost that is impractical for engineering applications.

This scale separation motivates the use of turbulence modeling. Rather than resolving every eddy, we can model the effect of unresolved scales on the resolved flow. The key insight from Kolmogorov's theory is that the small scales tend to be universal—they behave similarly regardless of the large-scale geometry. This universality is what makes turbulence modeling feasible: we need not know the exact details of every small eddy, only their statistical effect on the larger flow structures.

2.4 Turbulence Modeling Approaches

Three main approaches exist for simulating turbulent flows, differing in their treatment of the turbulent scales.

2.4.1 Direct Numerical Simulation (DNS)

DNS resolves all scales of turbulent motion by solving the Navier-Stokes equations without any turbulence modeling. The grid must be fine enough to capture the Kolmogorov scales, requiring:

$$N \sim Re^{9/4} \tag{2.15}$$

grid points in each direction for a three-dimensional simulation. This makes DNS computationally expensive and limits its application to relatively low Reynolds numbers and simple geometries. However, DNS provides the most accurate representation of turbulent flows and serves as a reference for validating turbulence models.

2.4.2 Reynolds-Averaged Navier-Stokes (RANS)

RANS solves for the time-averaged flow quantities, modeling all turbulent fluctuations through the Reynolds stress tensor. Common RANS models include:

- k-ε **model**: Two-equation model solving for turbulent kinetic energy k and dissipation rate ε
- k-ω **model**: Two-equation model using specific dissipation rate ω instead of ε
- **Reynolds Stress Models**: Solve transport equations for each component of the Reynolds stress tensor

RANS is computationally efficient but cannot capture unsteady turbulent phenomena or provide instantaneous flow information.

2.4.3 Large Eddy Simulation (LES)

LES represents a compromise between DNS and RANS. Large, energy-containing eddies are resolved directly while small-scale turbulence is modeled through a subgrid-scale (SGS) model. This approach is based on the observation that:

- Large eddies are geometry-dependent and carry most of the energy
- Small eddies are more universal and isotropic
- Modeling small scales introduces less error than modeling all scales

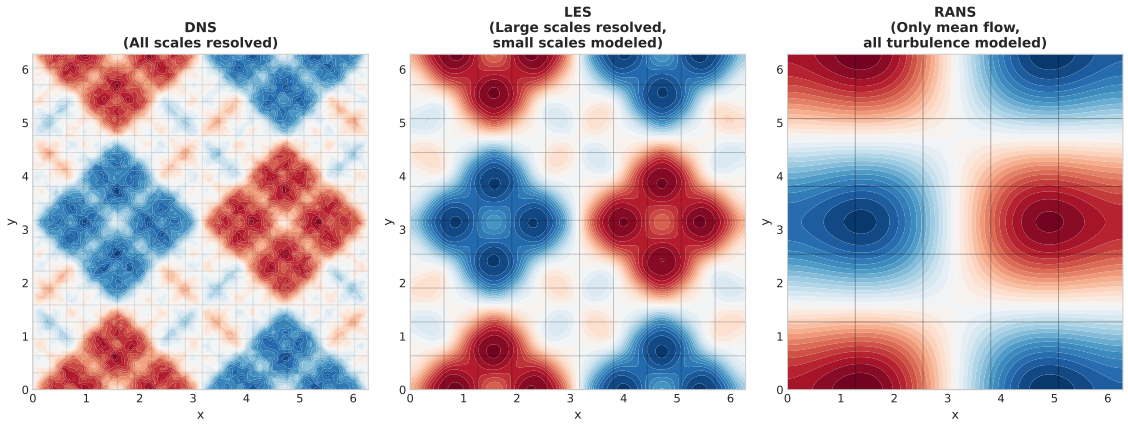

Figure 2.4: Comparison of DNS, LES, and RANS approaches for representing turbulent flow fields. DNS resolves all scales down to the Kolmogorov length, capturing every detail of the turbulent structures. LES resolves large-scale motions while modeling the effect of smaller scales. RANS captures only the time-averaged flow field, modeling all turbulent fluctuations through the Reynolds stress tensor.

Why LES for Engine Simulations? For internal combustion engine simulations, LES offers a compelling middle ground. The large-scale flow structures in engines—tumble, swirl, and squish motions—are highly geometry-dependent and vary from cycle to cycle. RANS, which predicts only the mean flow, cannot capture these cycle-to-cycle variations that significantly affect combustion variability. On the other hand, DNS remains computationally prohibitive for the high Reynolds numbers encountered in engines.

LES resolves the large, energy-containing eddies that dominate mixing and combustion processes while modeling the smaller, more universal scales. This allows LES to capture the unsteady, three-dimensional nature of engine flows at a computational cost that, while substantial, is achievable with modern high-performance computing resources. The challenge, particularly near walls, is ensuring that the subgrid-scale model accurately represents the unresolved physics—a challenge that motivates the enhanced viscosity approach developed in this work.

2.5 Large Eddy Simulation

The fundamental idea behind LES is elegant: rather than trying to resolve or model *all* turbulent scales, we resolve the large scales that are most important for engineering predictions and model only the small scales whose behavior is more universal. This section develops the mathematical framework for LES, starting with the filtering operation that separates resolved from modeled scales.

2.5.1 Spatial Filtering

The Filtering Concept: An Analogy Spatial filtering in LES can be understood through a simple analogy: imagine viewing a turbulent flow through a camera with limited resolution. The camera captures the large-scale features—the swirling vortices and bulk flow patterns—but blurs out the fine details smaller than a pixel. The filtered equations of LES describe what this "blurred" flow field does, while the subgrid-scale model accounts for the effect of the missing fine details.

Mathematically, we apply a low-pass filter to the Navier-Stokes equations. Large scales (wavelengths larger than the filter width) pass through unchanged, while small scales are removed and must be modeled. In LES, the flow variables are decomposed using a spatial filter rather than time averaging. For a variable ϕ, the filtered quantity $\tilde{\phi}$ is defined as:

$$\tilde{\phi}(\mathbf{x}, t) = \int_{\Omega} G(\mathbf{x} - \mathbf{x}', \Delta)\phi(\mathbf{x}', t)d\mathbf{x}' \tag{2.16}$$

where G is the filter kernel and Δ is the filter width. Common filter types include:

- **Box filter**: $G(\mathbf{x}) = 1/\Delta^3$ for $|x_i| \leq \Delta/2$
- **Gaussian filter**: $G(\mathbf{x}) = \left(\frac{6}{\pi\Delta^2}\right)^{3/2} \exp\left(-\frac{6|\mathbf{x}|^2}{\Delta^2}\right)$
- **Spectral cutoff filter**: Sharp cutoff in Fourier space

In practice, the grid itself often acts as an implicit filter with Δ related to the grid spacing.

2.5.2 Filtered Navier-Stokes Equations

Applying the filtering operation to the incompressible Navier-Stokes equations yields:

$$\frac{\partial \tilde{u}_i}{\partial x_i} = 0 \tag{2.17}$$

$$\frac{\partial \tilde{u}_i}{\partial t} + \frac{\partial (\tilde{u}_i \tilde{u}_j)}{\partial x_j} = -\frac{1}{\rho}\frac{\partial \tilde{p}}{\partial x_i} + \nu \frac{\partial^2 \tilde{u}_i}{\partial x_j \partial x_j} - \frac{\partial \tau_{ij}^{sgs}}{\partial x_j} \tag{2.18}$$

The subgrid-scale stress tensor τ_{ij}^{sgs} represents the effect of unresolved scales on the resolved flow:

$$\tau_{ij}^{sgs} = \widetilde{u_i u_j} - \tilde{u}_i \tilde{u}_j \tag{2.19}$$

2.5.3 Subgrid-Scale Models

The SGS stress tensor must be modeled to close the filtered equations. The most common approach uses the eddy viscosity concept:

$$\tau_{ij}^{sgs} - \frac{1}{3}\tau_{kk}^{sgs}\delta_{ij} = -2\nu_{sgs}\tilde{S}_{ij} \tag{2.20}$$

where $\tilde{S}_{ij}$ is the filtered strain rate tensor:

$$\tilde{S}_{ij} = \frac{1}{2}\left(\frac{\partial \tilde{u}_i}{\partial x_j} + \frac{\partial \tilde{u}_j}{\partial x_i}\right) \tag{2.21}$$

Smagorinsky Model

The Smagorinsky model relates the SGS viscosity to the local strain rate:

$$\nu_{sgs} = (C_s \Delta)^2 |\tilde{S}| \tag{2.22}$$

where $|\tilde{S}| = \sqrt{2\tilde{S}_{ij}\tilde{S}_{ij}}$ and C_s is the Smagorinsky constant, typically around 0.1–0.2. The model is simple but has limitations:

- Does not vanish at solid walls
- Cannot predict backscatter (energy transfer from small to large scales)
- Requires ad-hoc damping near walls

Dynamic Smagorinsky Model

Germano et al. proposed the dynamic procedure, which computes the model coefficient from the resolved scales during the simulation:

$$C_s^2 = \frac{\langle L_{ij} M_{ij} \rangle}{\langle M_{ij} M_{ij} \rangle} \tag{2.23}$$

where L_{ij} is the Leonard stress and M_{ij} involves the difference between strain rates at different filter levels. The angle brackets denote averaging over homogeneous directions or time.

WALE Model

The Wall-Adapting Local Eddy-viscosity (WALE) model provides correct near-wall behavior without explicit damping:

$$\nu_{sgs} = (C_w \Delta)^2 \frac{(S_{ij}^d S_{ij}^d)^{3/2}}{(\tilde{S}_{ij}\tilde{S}_{ij})^{5/2} + (S_{ij}^d S_{ij}^d)^{5/4}} \tag{2.24}$$

where S_{ij}^d is the traceless symmetric part of the square of the velocity gradient tensor.

2.6 Wall Treatment in LES

The near-wall region presents particular challenges for LES due to the small turbulent scales that develop close to solid boundaries. This section explains the physics of wall-bounded turbulence, why it is difficult to simulate, and the various approaches used to handle near-wall flows—culminating in the enhanced viscosity approach that forms the core of this thesis.

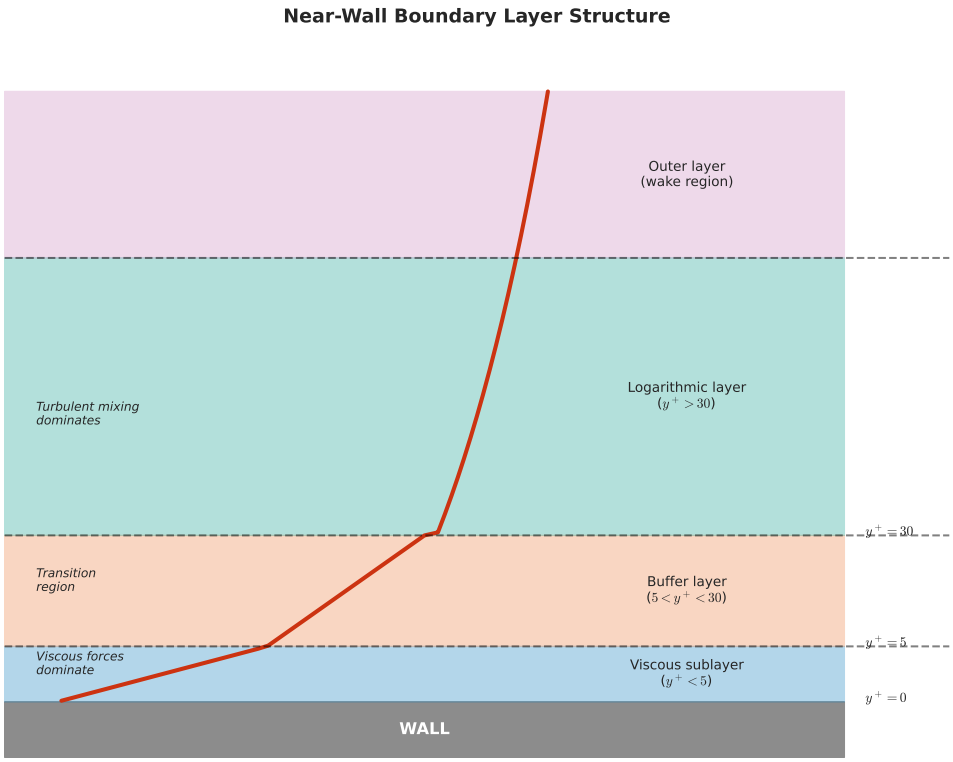

Figure 2.5: Structure of the turbulent boundary layer near a wall. Three distinct regions can be identified: the viscous sublayer ($y^+ < 5$) where viscous forces dominate and velocity varies linearly with distance; the buffer layer ($5 < y^+ < 30$) where both viscous and turbulent stresses are significant; and the logarithmic layer ($y^+ > 30$) where turbulent mixing dominates and velocity follows a logarithmic profile. The outer layer connects to the bulk flow.

2.6.1 Wall-Resolved LES

In wall-resolved LES, the grid is refined to capture the viscous sublayer and buffer layer directly. This requires:

- First grid point at $y^+ \approx 1$
- Grid spacing in wall-parallel directions: $\Delta x^+ \approx 50$–100, $\Delta z^+ \approx 15$–40

where the wall units are defined using the friction velocity $u_\tau = \sqrt{\tau_w/\rho}$:

$$y^+ = \frac{y u_\tau}{\nu}, \quad u^+ = \frac{u}{u_\tau} \tag{2.25}$$

2.6.2 Wall-Modeled LES

For high Reynolds number flows, wall-resolved LES becomes prohibitively expensive. Wall-modeled LES (WMLES) places the first grid point in the logarithmic layer ($y^+ > 30$) and

uses a wall model to represent the near-wall region.

Law of the Wall

The mean velocity profile near a smooth wall follows distinct regions:

- **Viscous sublayer** ($y^+ < 5$): $u^+ = y^+$
- **Buffer layer** ($5 < y^+ < 30$): Transition region
- **Logarithmic layer** ($y^+ > 30$): $u^+ = \frac{1}{\kappa}\ln(y^+) + B$

where $\kappa \approx 0.41$ is the von Kármán constant and $B \approx 5.2$ for smooth walls.

Why Classical Wall Functions Fail in Engines

Classical wall functions, derived from equilibrium boundary layer theory, assume that the flow near the wall is in local equilibrium—the production and dissipation of turbulent kinetic energy are balanced, and the boundary layer has had sufficient time to develop its characteristic structure. These assumptions break down in engine flows for several reasons:

1. **Rapid pressure changes:** During compression and expansion, the pressure changes by orders of magnitude over milliseconds. The boundary layer cannot reach equilibrium on such short timescales.
2. **Flow reversal and separation:** Near top dead center, the piston decelerates and reverses direction. The boundary layer on the piston surface experiences rapid changes in the wall shear stress, including possible flow reversal and reattachment.
3. **Non-zero pressure gradients:** The standard law of the wall assumes zero streamwise pressure gradient. In engines, strong favorable and adverse pressure gradients are the norm, significantly altering the boundary layer profile.
4. **Large-scale flow structures:** Tumble and swirl motions impose time-varying external conditions on the boundary layer that vary spatially across the combustion chamber surfaces.
5. **History effects:** The boundary layer at any instant depends on its entire history during the engine cycle, not just the instantaneous conditions. Equilibrium-based wall functions have no mechanism to account for this memory.

These limitations motivate the development of wall treatments that do not rely on equilibrium assumptions—such as the enhanced viscosity approach explored in this work.

Enhanced Viscosity Approach

One approach to wall modeling involves increasing the effective viscosity near the wall to account for unresolved turbulent transport. The total viscosity becomes:

$$\nu_{eff} = \nu + \nu_t^{wall} \tag{2.26}$$

where ν_t^{wall} is a modeled turbulent viscosity that captures the effect of unresolved near-wall eddies. This approach allows coarser grids near walls while maintaining the correct wall shear stress.

Physical Mechanism of Enhanced Viscosity The enhanced viscosity approach can be understood through a physical lens. Near a wall, the turbulent eddies that would normally transport momentum are suppressed by the wall's presence—they are "squashed" and cannot extend beyond the wall. On a coarse LES grid that does not resolve these near-wall eddies, their momentum transport effect is missing.

By locally increasing the viscosity, we are effectively saying: "The unresolved turbulent fluctuations would have mixed momentum across this region. Since we cannot resolve them, we will increase the diffusion coefficient (viscosity) so that the resolved equations produce the correct net momentum transport." This is analogous to how eddy viscosity models work in general, but specifically tuned for the near-wall region where the turbulence structure is known from boundary layer theory.

The advantage of this approach for engine simulations is that it does not assume equilibrium—the enhanced viscosity simply provides additional diffusion that mimics unresolved turbulent transport, regardless of whether the flow is accelerating, decelerating, or experiencing pressure gradients.

2.7 Channel Flow

The plane channel flow serves as a canonical test case for wall-bounded turbulence studies due to its geometric simplicity and well-documented behavior. Before attempting to simulate the complex, transient flows in an engine, it is essential to validate the wall treatment approach in a controlled environment where analytical and high-fidelity DNS data are available for comparison.

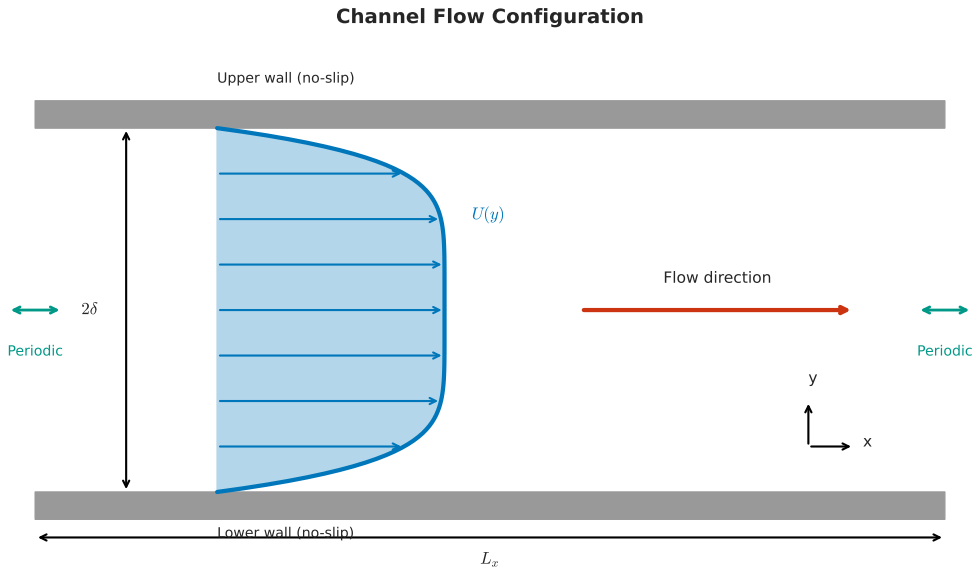

Figure 2.6: Plane channel flow configuration. The flow is driven by a pressure gradient between two parallel plates separated by distance 2δ. Periodic boundary conditions are applied in the streamwise direction, and the flow is statistically homogeneous in both streamwise and spanwise directions. The mean velocity profile $U(y)$ develops a characteristic turbulent shape with thin boundary layers near each wall.

2.7.1 Configuration

The flow is driven by a pressure gradient between two parallel infinite plates separated by a distance $2h$ (or 2δ, using the half-channel height as the reference length). The flow is statistically steady and homogeneous in the streamwise (x) and spanwise (z) directions. This homogeneity allows averaging over these directions to obtain smooth statistical profiles with relatively short simulation times.

Why Channel Flow for Validation? Channel flow offers several advantages for validating wall models:

- **Simple geometry:** The flat parallel walls eliminate geometric complexity, isolating the wall treatment behavior.
- **Well-known physics:** Decades of experimental and DNS studies have established accurate reference data.
- **Statistical convergence:** Spatial averaging in homogeneous directions accelerates convergence of turbulent statistics.
- **Controlled conditions:** The steady-state, equilibrium nature allows direct comparison with law-of-the-wall predictions.

By validating the enhanced viscosity wall model first in channel flow, we establish confidence in its behavior before applying it to the more challenging engine environment.

2.7.2 Friction Reynolds Number

The friction Reynolds number characterizes the flow:

$$Re_\tau = \frac{u_\tau h}{\nu} \tag{2.27}$$

where $u_\tau = \sqrt{\tau_w/\rho}$ is the friction velocity based on the wall shear stress τ_w. This Reynolds number represents the ratio of the outer length scale h to the viscous length scale ν/u_τ.

2.7.3 Mean Velocity Profile

In wall units, the mean velocity profile exhibits the classical law of the wall behavior. The friction velocity is related to the pressure gradient by:

$$\tau_w = -h\frac{dp}{dx} \tag{2.28}$$

2.7.4 Turbulent Statistics

Key quantities for characterizing turbulent channel flow include:

- Reynolds stresses: $\overline{u_i' u_j'}$
- Turbulent kinetic energy: $k = \frac{1}{2}\overline{u_i' u_i'}$
- Root-mean-square velocity fluctuations: $u^+_{rms} = \sqrt{\overline{u'^2}}/u_\tau$

These statistics, when obtained from DNS, serve as reference data for validating LES with various wall treatments.

2.8 Immersed Boundary Methods

Immersed boundary methods provide an alternative to body-fitted grids for simulating flows around complex geometries. The solid boundaries are represented on a fixed Cartesian grid, which simplifies grid generation and enables efficient handling of moving boundaries.

2.8.1 Concept and Motivation

In traditional body-fitted approaches, the computational grid conforms to the solid boundaries, requiring complex mesh generation and potential mesh quality issues near curved surfaces.

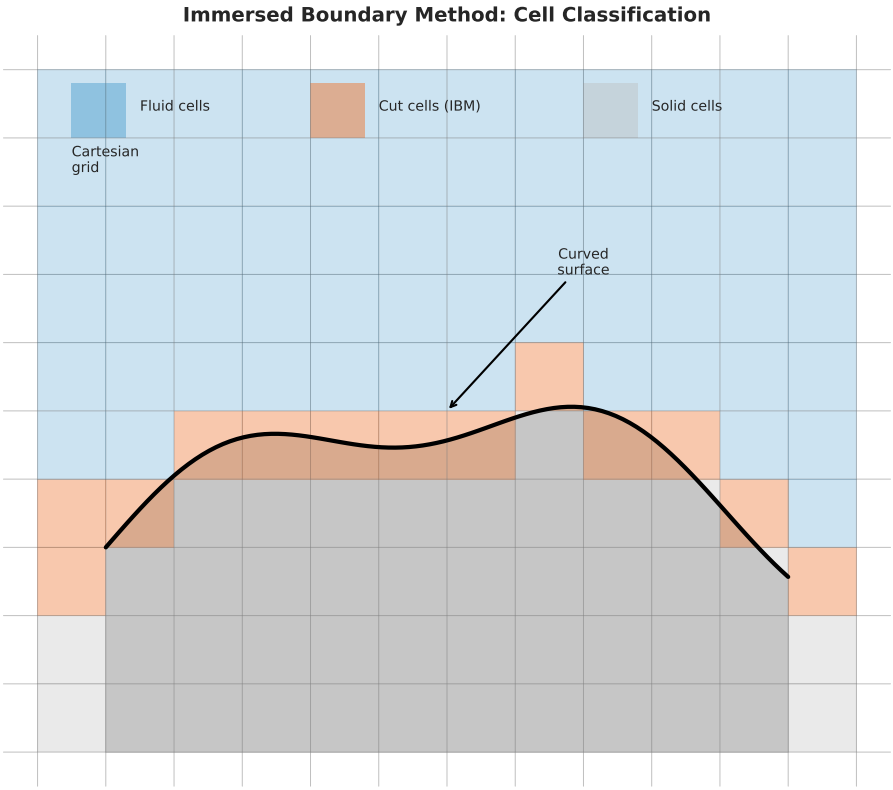

Figure 2.7: Immersed boundary method concept. A curved solid surface is represented on a fixed Cartesian grid. Cells are classified as fluid cells (where the Navier-Stokes equations are solved normally), solid cells (inside the body), or cut cells (intersected by the boundary). Special treatment is applied at cut cells to enforce the boundary conditions.

Immersed boundary methods instead use a simple background grid (typically Cartesian) and impose boundary conditions through additional forcing terms or modified discretization near the immersed surface.

The key advantages include:

- Simple grid generation regardless of geometry complexity
- Efficient handling of moving boundaries without remeshing
- Straightforward parallelization on structured grids
- Natural extension to multi-body problems

2.8.2 Classification of Methods

Immersed boundary methods can be classified into two main categories:

Continuous Forcing Approach

The original immersed boundary method by Peskin adds a forcing term to the momentum equations:

$$\frac{\partial \mathbf{u}}{\partial t} + (\mathbf{u} \cdot \nabla)\mathbf{u} = -\frac{1}{\rho}\nabla p + \nu \nabla^2 \mathbf{u} + \mathbf{f}_{IB} \tag{2.29}$$

where $\mathbf{f}_{IB}$ is the immersed boundary forcing that enforces the desired velocity at the boundary. This forcing is distributed to the grid using a smoothed delta function.

Discrete Forcing Approach

Direct forcing methods modify the discrete equations near the boundary. The velocity at boundary points is directly set or interpolated to satisfy the boundary condition:

$$u_{IB} = u_{desired} \tag{2.30}$$

This approach provides sharper boundary representation and is well-suited for high Reynolds number flows.

2.8.3 Wall Treatment with Immersed Boundaries

Combining wall treatment with immersed boundaries requires special consideration. The wall model must:

- Identify cells cut by the immersed boundary
- Compute the wall distance for each affected cell
- Apply the appropriate wall treatment based on the local y^+
- Ensure smooth transition to the outer flow region

The enhanced viscosity approach is particularly compatible with immersed boundaries because it modifies a local property (viscosity) rather than imposing explicit velocity boundary conditions.

2.9 Internal Combustion Engine Flows

The flow within an internal combustion engine exhibits unique characteristics that distinguish it from canonical turbulent flows. Understanding these characteristics is essential for developing appropriate simulation strategies and wall treatments.

2.9.1 Engine Cycle and Flow Phases

A four-stroke engine cycle comprises distinct phases with different flow characteristics. Figure 2.8 illustrates the four strokes and their associated flow patterns.

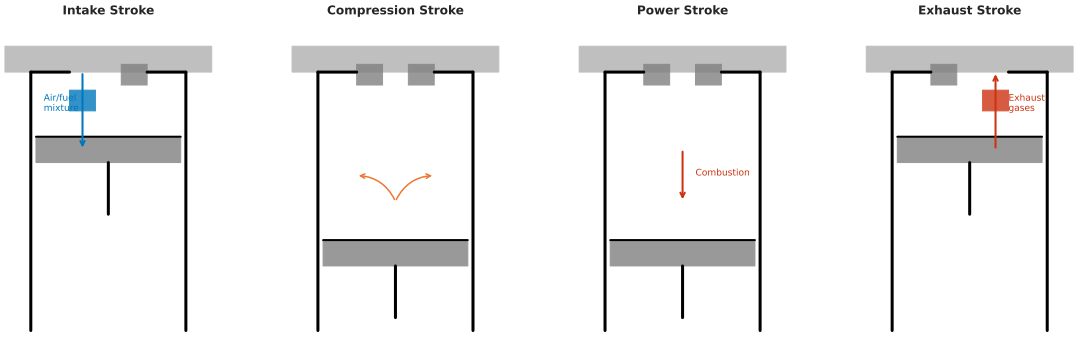

Figure 2.8: The four strokes of an internal combustion engine cycle. During intake, fresh charge enters through the open intake valve, generating large-scale vortical structures. Compression increases pressure and temperature while modifying the flow structures. The power stroke follows combustion, with expansion driving the piston. Finally, exhaust gases are expelled through the open exhaust valve.

Intake Stroke

During intake, the piston moves downward, creating a pressure difference that draws fresh charge through the intake valve. The flow entering the cylinder forms a high-velocity jet that generates large-scale vortical structures.

Compression Stroke

As the piston moves upward, the in-cylinder gases are compressed. The large-scale structures generated during intake are modified by the changing volume and interact with the walls.

Expansion Stroke

Following combustion, the piston is driven downward by the expanding gases. The boundary layers on the piston and cylinder walls experience rapid changes in pressure and temperature.

Exhaust Stroke

The piston moves upward to expel the combustion products through the exhaust valve.

2.9.2 Large-Scale Flow Structures

Engine designers use intake port geometry to generate organized large-scale motions that enhance mixing and combustion. These structures, illustrated in Figure 2.9, play a crucial role in determining combustion efficiency and emissions.

Tumble

Tumble is a large-scale rotational motion about an axis perpendicular to the cylinder axis. It is generated by directing the intake flow toward one side of the combustion chamber.

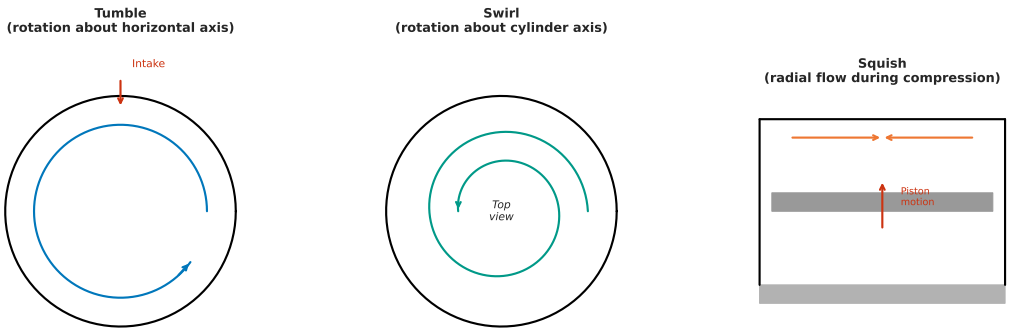

Figure 2.9: Large-scale organized flow motions in internal combustion engines. **Tumble** is rotation about a horizontal axis perpendicular to the cylinder axis, generated by directing intake flow toward one side of the chamber. **Swirl** is rotation about the cylinder axis, created by tangential intake flow. **Squish** is the radial flow generated when the piston approaches the cylinder head during compression.

As compression proceeds, the tumble vortex is compressed and eventually breaks down into smaller-scale turbulence, enhancing the mixing before ignition.

Swirl

Swirl is rotation about the cylinder axis, generated by tangential entry of the intake flow. Swirl persists longer than tumble due to the axial symmetry and can enhance mixing during combustion.

Squish

Squish is the radial flow generated as the piston approaches the cylinder head, forcing gases from the periphery toward the center (or vice versa). Squish enhances turbulence near top dead center.

2.9.3 Non-Equilibrium Boundary Layers

Engine boundary layers differ from classical equilibrium boundary layers in several important aspects:

Pressure Gradient Effects

The rapid pressure changes during compression and expansion create strong favorable and adverse pressure gradients that affect boundary layer development:

- Favorable gradients (during expansion) thin the boundary layer
- Adverse gradients (during compression) thicken the boundary layer and can cause separation

Unsteady Effects

The boundary layer does not have time to reach equilibrium between the different phases of the engine cycle. The wall shear stress lags behind the bulk flow changes.

History Effects

The boundary layer at any instant depends on the flow history, not just the instantaneous conditions. This makes equilibrium-based wall functions unreliable.

2.10 Optical Engines

Optical engines are research engines equipped with transparent components that allow visual access to the combustion chamber for laser-based measurements.

2.10.1 Design Features

Typical optical engine features include:

- Extended piston with quartz or sapphire window in the crown
- Transparent cylinder liner (quartz)
- Mirror below the piston for through-piston imaging
- Skip-firing operation to protect optical components

2.10.2 Research Applications

Optical engines enable:

- Particle Image Velocimetry (PIV) for velocity field measurement
- Laser-Induced Fluorescence (LIF) for species concentration
- High-speed imaging of combustion
- Validation data for CFD simulations

2.10.3 Limitations

Optical engine measurements have limitations:

- Lower firing rates than production engines
- Optical access constraints limit geometry modifications
- Skip-firing affects cycle-to-cycle variations

Despite these limitations, optical engines provide valuable data for understanding in-cylinder processes and validating simulation methods.

2.11 The PsiPhi Solver

PsiPhi is an in-house computational fluid dynamics code developed at the University of Duisburg-Essen, primarily for the simulation of turbulent reacting flows. The solver has been applied to a wide range of combustion and engine-related problems.

2.11.1 Development History

PsiPhi originated from research activities at the Chair of Fluid Dynamics, with a focus on high-performance computing approaches for turbulent flow simulation. The code has been continuously developed and validated against experimental and benchmark data.

2.11.2 Key Features

The main characteristics of PsiPhi include:

- Structured Cartesian grid approach for computational efficiency
- Support for both DNS and LES
- Immersed boundary method for complex geometry handling
- Scalable parallelization for high-performance computing clusters
- Various subgrid-scale models for LES
- Combustion modeling capabilities for reacting flows

2.11.3 Solver Approach

PsiPhi solves the incompressible Navier-Stokes equations using a finite volume discretization on a staggered grid. The pressure-velocity coupling is handled through a projection method (fractional step), ensuring mass conservation at each time step.

The use of structured Cartesian grids enables:

- Efficient memory access patterns
- Simple implementation of high-order schemes
- Straightforward domain decomposition for parallelization
- Compatibility with immersed boundary methods for complex geometries

2.11.4 Application Areas

PsiPhi has been applied to various flow configurations:

- Turbulent jet flames and diffusion flames
- Premixed combustion
- Internal combustion engine simulations
- Fundamental turbulence studies

The combination of structured grids, immersed boundaries, and established turbulence modeling makes PsiPhi well-suited for the engine boundary layer studies in this work.

3. Numerical Methods

This chapter describes the numerical methods employed in this work, with particular focus on the in-house solver PsiPhi used for both DNS and LES simulations. The discretization schemes, time integration methods, and implementation of the wall treatment are presented.

3.1 The PsiPhi Solver

PsiPhi is an in-house computational fluid dynamics solver developed for the simulation of turbulent reacting flows. The solver is designed for high-performance computing environments and supports both DNS and LES approaches.

3.1.1 Governing Equations

PsiPhi solves the incompressible Navier-Stokes equations in their filtered form for LES or unfiltered form for DNS:

$$\frac{\partial u_i}{\partial x_i} = 0 \tag{3.1}$$

$$\frac{\partial u_i}{\partial t} + \frac{\partial (u_i u_j)}{\partial x_j} = -\frac{1}{\rho}\frac{\partial p}{\partial x_i} + \frac{\partial}{\partial x_j}\left[(\nu + \nu_t)\left(\frac{\partial u_i}{\partial x_j} + \frac{\partial u_j}{\partial x_i}\right)\right] + f_i \tag{3.2}$$

where ν_t represents the turbulent viscosity, which is zero for DNS and computed from an SGS model for LES.

3.2 Spatial Discretization

3.2.1 Finite Volume Method

PsiPhi employs the Finite Volume Method (FVM) for spatial discretization. The computational domain is divided into control volumes, and the governing equations are integrated over each control volume. For a general transport equation:

$$\frac{\partial \phi}{\partial t} + \nabla \cdot (\mathbf{u}\phi) = \nabla \cdot (\Gamma \nabla \phi) + S_\phi \tag{3.3}$$

the integration over a control volume V with surface A yields:

$$\frac{\partial}{\partial t}\int_V \phi \, dV + \oint_A (\mathbf{u}\phi) \cdot d\mathbf{A} = \oint_A (\Gamma \nabla \phi) \cdot d\mathbf{A} + \int_V S_\phi \, dV \tag{3.4}$$

3.2.2 Grid Arrangement

The solver uses a staggered grid arrangement where:

- Scalar quantities (pressure, temperature) are stored at cell centers
- Velocity components are stored at cell faces

This arrangement prevents the checkerboard pressure oscillations that can occur with collocated grids and ensures strong pressure-velocity coupling.

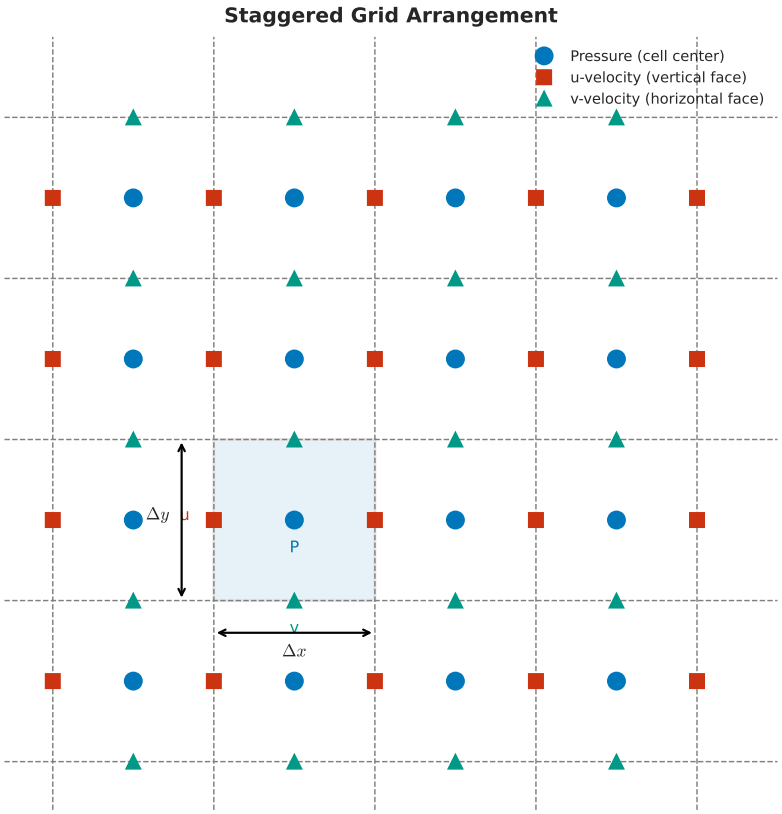

Figure 3.1: Staggered grid arrangement used in PsiPhi. Pressure is stored at cell centers (circles), while velocity components are stored at cell faces: u-velocity at vertical faces (squares) and v-velocity at horizontal faces (triangles). This arrangement naturally couples pressure and velocity, preventing numerical oscillations.

Why Staggered Grids? The choice of a staggered grid arrangement deserves explanation, as it impacts how the equations are discretized and how boundary conditions are applied. On a collocated grid (where all variables are stored at the same location), the pressure gradient is computed using values two cells apart. This can lead to a decoupling where alternating high and low pressures satisfy the discrete equations equally well—the infamous "checkerboard" pattern.

On a staggered grid, the pressure gradient acting on a velocity component uses pressure values from immediately adjacent cells, creating a tight coupling. When we compute u at a face, we use pressures from the cells on either side of that face. This direct connection eliminates the checkerboard problem and provides robust pressure-velocity coupling without requiring additional stabilization techniques.

3.2.3 Convective Term Discretization

The convective fluxes are discretized using a combination of schemes depending on the application:

Central Differencing Scheme

For DNS and well-resolved LES, the central differencing scheme (CDS) provides second-order accuracy:

$$\phi_f = \frac{\phi_P + \phi_N}{2} \tag{3.5}$$

where ϕ_f is the face value, and ϕ_P and ϕ_N are the values at the neighboring cell centers.

Upwind Scheme

For stability in convection-dominated flows, the upwind scheme can be employed:

$$\phi_f = \begin{cases} \phi_P & \text{if } (\mathbf{u} \cdot \mathbf{n})_f > 0 \\ \phi_N & \text{if } (\mathbf{u} \cdot \mathbf{n})_f < 0 \end{cases} \tag{3.6}$$

TVD Schemes

Total Variation Diminishing (TVD) schemes provide a balance between accuracy and stability by using flux limiters. The face value is computed as:

$$\phi_f = \phi_P + \frac{1}{2}\psi(r)(\phi_N - \phi_P) \tag{3.7}$$

where $\psi(r)$ is a limiter function and r is the ratio of consecutive gradients.

Choosing the Right Scheme: A Practical Guide The choice between these discretization schemes depends on the simulation type and the trade-offs between accuracy and stability:

- **Central Differencing (CDS)**: Use for DNS and well-resolved LES where the grid is fine enough to capture all relevant scales. CDS is second-order accurate and does not introduce numerical diffusion, making it ideal for capturing the energy cascade accurately. However, CDS can become unstable on coarse grids or in regions of strong gradients.
- **Upwind**: Use when stability is paramount, such as in coarse RANS simulations or regions with very strong convection. Upwind is unconditionally stable but introduces numerical diffusion that can smear gradients and artificially dissipate turbulent structures. For turbulence simulations, this artificial dissipation is generally unacceptable.

- **TVD Schemes**: Use when you need a balance—for example, in LES on moderately resolved grids or in regions where CDS produces spurious oscillations. TVD schemes adapt locally: they behave like CDS in smooth regions (preserving accuracy) and switch toward upwind near sharp gradients (ensuring stability). The limiter function $\psi(r)$ controls this transition.

For the channel flow simulations in this work, CDS is used throughout, as the grid resolution is sufficient to maintain stability while preserving the accuracy needed for turbulence statistics.

3.2.4 Diffusive Term Discretization

The diffusive fluxes are discretized using central differencing:

$$\left(\Gamma \frac{\partial \phi}{\partial x}\right)_f = \Gamma_f \frac{\phi_N - \phi_P}{\Delta x} \tag{3.8}$$

For non-orthogonal grids, correction terms are added to maintain accuracy.

3.3 Pressure-Velocity Coupling

The incompressible Navier-Stokes equations present a numerical challenge: the pressure does not appear in the continuity equation explicitly, yet it must adjust instantaneously to ensure the velocity field remains divergence-free. This coupling between pressure and velocity requires special treatment.

3.3.1 Projection Method

The Physical Picture Before diving into the mathematics, it helps to understand the physical role of pressure. In incompressible flow, pressure is not a thermodynamic variable (as it would be in compressible flow) but rather a Lagrange multiplier that enforces the incompressibility constraint. The pressure adjusts to whatever value is needed to keep the velocity field divergence-free.

The projection method exploits this by splitting the time advancement into two stages:

1. First, we advance the velocity using the momentum equation but ignore pressure. This gives an intermediate velocity field that generally does not satisfy continuity.
2. Second, we compute a pressure field that "projects" this intermediate velocity onto the space of divergence-free fields. The result is a velocity that satisfies both momentum and continuity.

PsiPhi uses a fractional step (projection) method to enforce the incompressibility constraint. The algorithm proceeds as follows:

Step 1: Predictor step

Compute an intermediate velocity u_i^* by solving the momentum equation without the pressure gradient:

$$\frac{u_i^* - u_i^n}{\Delta t} = -\frac{\partial (u_i u_j)^n}{\partial x_j} + \nu \frac{\partial^2 u_i^n}{\partial x_j \partial x_j} + f_i \tag{3.9}$$

Step 2: Pressure Poisson equation

The pressure is obtained by solving a Poisson equation derived from the continuity constraint:

$$\nabla^2 p^{n+1} = \frac{\rho}{\Delta t} \nabla \cdot \mathbf{u}^* \tag{3.10}$$

Step 3: Corrector step

The velocity is corrected to satisfy continuity:

$$u_i^{n+1} = u_i^* - \frac{\Delta t}{\rho} \frac{\partial p^{n+1}}{\partial x_i} \tag{3.11}$$

Why This Works The key insight is that any vector field can be decomposed into a divergence-free (solenoidal) part and a curl-free (irrotational) part—the Helmholtz decomposition. The intermediate velocity $\mathbf{u}^*$ contains both components. The pressure gradient ∇p is curl-free by definition. By subtracting the right pressure gradient from $\mathbf{u}^*$, we remove exactly the curl-free component that violates continuity, leaving only the divergence-free part.

The Poisson equation for pressure (Eq. 3.10) is derived by taking the divergence of the corrector step and requiring $\nabla \cdot \mathbf{u}^{n+1} = 0$. This elegant mathematical structure ensures that the algorithm maintains mass conservation to machine precision.

3.3.2 Poisson Solver

The pressure Poisson equation is solved using iterative methods. PsiPhi supports:

- Jacobi iteration
- Gauss-Seidel iteration
- Successive Over-Relaxation (SOR)
- Conjugate Gradient methods
- Multigrid acceleration

3.4 Temporal Discretization

3.4.1 Explicit Time Integration

For the convective and source terms, explicit time integration schemes are employed:

Euler Method

The first-order Euler method:

$$\phi^{n+1} = \phi^n + \Delta t \cdot F(\phi^n) \tag{3.12}$$

Runge-Kutta Methods

Higher-order accuracy is achieved using Runge-Kutta schemes. The third-order Runge-Kutta (RK3) method:

$$\phi^{(1)} = \phi^n + \Delta t \cdot F(\phi^n) \tag{3.13}$$

$$\phi^{(2)} = \frac{3}{4}\phi^n + \frac{1}{4}\phi^{(1)} + \frac{1}{4}\Delta t \cdot F(\phi^{(1)}) \tag{3.14}$$

$$\phi^{n+1} = \frac{1}{3}\phi^n + \frac{2}{3}\phi^{(2)} + \frac{2}{3}\Delta t \cdot F(\phi^{(2)}) \tag{3.15}$$

3.4.2 Time Step Restriction

The time step is limited by stability constraints:

CFL Condition

The Courant-Friedrichs-Lewy (CFL) condition for convective stability:

$$\Delta t \leq \text{CFL} \cdot \min\left(\frac{\Delta x}{|u|}, \frac{\Delta y}{|v|}, \frac{\Delta z}{|w|}\right) \tag{3.16}$$

where $\text{CFL} \leq 1$ for explicit schemes.

Viscous Stability

The diffusive stability constraint:

$$\Delta t \leq \frac{\Delta x^2}{2\nu} \tag{3.17}$$

3.5 Boundary Conditions

3.5.1 Inlet Boundary

At inlet boundaries, velocity components are prescribed:

$$u_i = u_{i,\text{inlet}} \tag{3.18}$$

For turbulent inflow, synthetic turbulence generators or recycling methods can be employed.

3.5.2 Outlet Boundary

Convective outflow conditions allow disturbances to exit the domain:

$$\frac{\partial \phi}{\partial t} + U_c \frac{\partial \phi}{\partial n} = 0 \tag{3.19}$$

where U_c is the convection velocity and n is the outward normal direction.

3.5.3 Wall Boundary

At solid walls, the no-slip condition is applied:

$$u_i = 0 \tag{3.20}$$

For the pressure, a zero normal gradient condition is used:

$$\frac{\partial p}{\partial n} = 0 \tag{3.21}$$

3.5.4 Periodic Boundary

For channel flow simulations, periodic boundary conditions are applied in the streamwise and spanwise directions:

$$\phi(x) = \phi(x + L_x), \quad \phi(z) = \phi(z + L_z) \tag{3.22}$$

3.6 Immersed Boundary Implementation

PsiPhi uses an immersed boundary method to represent complex geometries on the Cartesian grid. This section describes the implementation details.

3.6.1 Geometry Representation

The solid geometry is represented using a signed distance function $\phi(\mathbf{x})$:

$$\phi(\mathbf{x}) = \begin{cases} > 0 & \text{fluid region} \\ = 0 & \text{boundary surface} \\ < 0 & \text{solid region} \end{cases} \tag{3.23}$$

The distance function is computed from the CAD geometry (typically STL format) and stored on the grid. For moving boundaries, the distance function is updated at each time step.

3.6.2 Cell Classification

Grid cells are classified based on the signed distance function:

- **Fluid cells**: Entirely in the fluid region ($\phi > 0$ at all vertices)
- **Solid cells**: Entirely in the solid region ($\phi < 0$ at all vertices)
- **Cut cells**: Intersected by the boundary (mixed signs at vertices)

Cut cells require special treatment to enforce boundary conditions while maintaining conservation.

3.6.3 Velocity Boundary Conditions

The no-slip condition at immersed boundaries is enforced through direct forcing. For a cut cell, the velocity is interpolated to satisfy:

$$u_{IB} = u_{wall} + (u_{fluid} - u_{wall}) \cdot f(\phi) \tag{3.24}$$

where $f(\phi)$ is a blending function based on the distance to the wall.

For moving boundaries such as the piston, the wall velocity u_{wall} corresponds to the local surface velocity.

3.6.4 Pressure Treatment

The pressure in solid cells is extrapolated from the fluid region to ensure smooth pressure gradients across the immersed boundary:

$$\left.\frac{\partial p}{\partial n}\right|_{wall} = 0 \tag{3.25}$$

This Neumann condition is consistent with the no-penetration constraint at solid walls.

3.7 LES Implementation

3.7.1 Subgrid-Scale Model

For LES, PsiPhi implements the Smagorinsky model with the SGS viscosity:

$$\nu_{sgs} = (C_s \Delta)^2 |\tilde{S}| \tag{3.26}$$

where $\Delta = (\Delta x \cdot \Delta y \cdot \Delta z)^{1/3}$ is the filter width based on the local grid spacing.

3.7.2 Near-Wall Treatment

Near solid walls, the Smagorinsky model requires damping to account for the reduced turbulent length scales. The van Driest damping function is applied:

$$f_d = 1 - \exp\left(-\frac{y^+}{A^+}\right) \tag{3.27}$$

where $A^+ \approx 25$ is the damping constant.

3.8 Wall Treatment: Enhanced Molecular Viscosity Approach

The primary focus of this work is the development of a novel wall treatment for LES that accounts for boundary-layer effects by introducing a locally increased molecular viscosity near the walls. This approach is specifically designed for use with immersed boundaries.

3.8.1 Motivation

Classical wall functions fail under the rapidly changing and non-equilibrium conditions of internal combustion engines. The enhanced molecular viscosity approach offers several advantages:

- Does not assume equilibrium boundary layer profiles
- Compatible with immersed boundary methods
- Computationally efficient for complex moving geometries
- Can be calibrated and verified against standard wall functions

3.8.2 Formulation

The effective viscosity in the near-wall region is modified to account for unresolved turbulent transport:

$$\nu_{eff}(y) = \nu \cdot (1 + \alpha \cdot f(y/\delta)) \tag{3.28}$$

where:

- ν is the molecular (kinematic) viscosity
- α is the enhancement factor (to be determined)
- $f(y/\delta)$ is a profile function depending on wall distance
- δ is a characteristic length scale (boundary layer thickness or cell size)

The key distinction from turbulent viscosity models is that this approach directly manipulates the molecular viscosity coefficient, which governs the diffusive fluxes in the momentum equation.

3.8.3 1D Model Development

A one-dimensional model is developed to determine the viscosity profile across the boundary layer. The 1D model solves a simplified momentum balance in the wall-normal direction:

$$\frac{d}{dy}\left(\nu_{eff}(y)\frac{du}{dy}\right) = \frac{1}{\rho}\frac{dp}{dx} \tag{3.29}$$

This equation is integrated from the wall to the edge of the boundary layer to obtain the velocity profile and wall shear stress. The viscosity profile $\nu_{eff}(y)$ is adjusted to match the law of the wall behavior.

3.8.4 Verification Strategy

The model is verified using standard wall functions. For equilibrium boundary layers, the enhanced viscosity model should reproduce:

- Linear velocity profile in the viscous sublayer: $u^+ = y^+$
- Logarithmic profile in the log layer: $u^+ = \frac{1}{\kappa}\ln(y^+) + B$
- Correct wall shear stress: $\tau_w = \mu \frac{\partial u}{\partial y}\Big|_{wall}$

The verification ensures that the model recovers classical results before application to non-equilibrium engine flows.

3.8.5 Implementation in PsiPhi

The enhanced viscosity is implemented by modifying the diffusive term in the momentum equation for cells near immersed boundaries:

Step 1: Wall Distance Computation

For each cell near an immersed boundary, the wall distance y is computed from the signed distance function.

Step 2: Viscosity Enhancement

The local viscosity is modified according to:

$$\nu_{cell} = \nu \cdot \left(1 + \alpha \cdot f\left(\frac{y}{\Delta}\right)\right) \tag{3.30}$$

where Δ is the local grid spacing.

Step 3: Blending

A smooth transition to the standard LES viscosity is applied:

$$\nu_{total} = \nu_{cell} + \nu_{sgs} \tag{3.31}$$

The blending function f approaches zero far from the wall, ensuring that the standard LES behavior is recovered in the bulk flow.

3.8.6 Coupling with Immersed Boundaries

The enhanced viscosity wall treatment is naturally coupled with the immersed boundary method:

- The signed distance function provides the wall distance
- Cut cells receive the enhanced viscosity based on their distance to the surface
- Moving boundaries automatically update the wall distance
- No special grid requirements near the wall

This coupling enables consistent treatment of all solid surfaces in the engine, including the moving piston.

3.9 Channel Flow Configuration

3.9.1 Computational Domain

The channel flow simulations use a domain of size $L_x \times L_y \times L_z$ with:

- $L_x = 2\pi h$ in the streamwise direction
- $L_y = 2h$ in the wall-normal direction (channel half-height h)
- $L_z = \pi h$ in the spanwise direction

3.9.2 Grid Requirements

For DNS, the grid resolution must satisfy:

- $\Delta x^+ \approx 10$–15 (streamwise)
- $\Delta y^+_{wall} < 1$ (first cell at wall)
- $\Delta z^+ \approx 5$–10 (spanwise)

For LES with wall treatment:

- $\Delta x^+ \approx 50$–100 (streamwise)
- $\Delta y^+_{wall} \approx 1$–$30$ depending on wall model
- $\Delta z^+ \approx 20$–50 (spanwise)

3.9.3 Flow Driving

The channel flow is driven by a constant pressure gradient in the streamwise direction. The pressure gradient is related to the target friction Reynolds number:

$$\frac{dp}{dx} = -\frac{\rho u_\tau^2}{h} = -\frac{\rho \nu^2 Re_\tau^2}{h^3} \tag{3.32}$$

3.10 Post-Processing and Statistics

3.10.1 Temporal Averaging

Statistical quantities are computed by time-averaging over a sufficiently long period after the flow has reached a statistically steady state:

$$\langle \phi \rangle = \frac{1}{T} \int_0^T \phi(t)\, dt \tag{3.33}$$

3.10.2 Spatial Averaging

For channel flow, additional averaging is performed over the homogeneous directions (streamwise and spanwise):

$$\langle \phi \rangle_{xz} = \frac{1}{L_x L_z} \int_0^{L_x} \int_0^{L_z} \phi(x, y, z)\, dx\, dz \tag{3.34}$$

3.10.3 Computed Quantities

The following quantities are extracted for comparison:

- Mean velocity: $\langle u \rangle^+ = \langle u \rangle / u_\tau$
- Velocity fluctuations: $u^+_{rms} = \sqrt{\langle u'^2 \rangle} / u_\tau$
- Reynolds shear stress: $\langle u'v' \rangle^+ = \langle u'v' \rangle / u_\tau^2$
- Turbulent kinetic energy: $k^+ = k / u_\tau^2$

4. CAD Model and Engine Geometry

This chapter presents the CAD model development for the optical engine used in this study. The engine geometry is based on the University of Duisburg-Essen optical research engine, a facility designed to provide optical access for laser-based diagnostics while maintaining realistic engine operating conditions.

4.1 The Optical Engine Facility

4.1.1 Overview

The optical engine at the University of Duisburg-Essen is an AVL 5811 single-cylinder research engine specifically designed for fundamental studies of in-cylinder flow and combustion processes. The transparent components allow researchers to apply advanced laser-based measurement techniques such as Particle Image Velocimetry (PIV) and Laser-Induced Fluorescence (LIF) to study the flow field and species distributions within the combustion chamber.

4.1.2 Engine Specifications

The key specifications of the optical engine are summarized in Table 4.1.

Table 4.1: Specifications of the AVL 5811 optical engine.

Parameter	**Value**
Engine type	Single-cylinder, four-stroke
Bore	84 mm
Stroke	90 mm
Displacement	499 cm^3
Connecting rod length	161 mm
Compression ratio	∼10:1
Valve configuration	4-valve pentroof
Nominal speed	3000 rpm
Optical access	Piston crown (sapphire), cylinder liner (quartz)

4.1.3 Optical Access Features

The engine provides optical access through several transparent components:

- **Extended piston with quartz window:** A Bowditch-type extended piston design allows a mirror to be placed below the piston, enabling through-piston imaging of the combustion chamber from below. The piston crown contains a large quartz window.
- **Quartz cylinder liner:** A section of the cylinder liner is made from fused quartz, providing lateral optical access. This enables side-view imaging and laser sheet illumination for PIV measurements.
- **Pentroof window:** Small windows in the pentroof provide additional access angles for laser diagnostics.

These optical access features impose constraints on the engine design—the quartz components have different thermal properties than metal, and the extended piston increases the effective

crank-slider mechanism length. However, the geometric similarity to production engines is maintained as closely as possible.

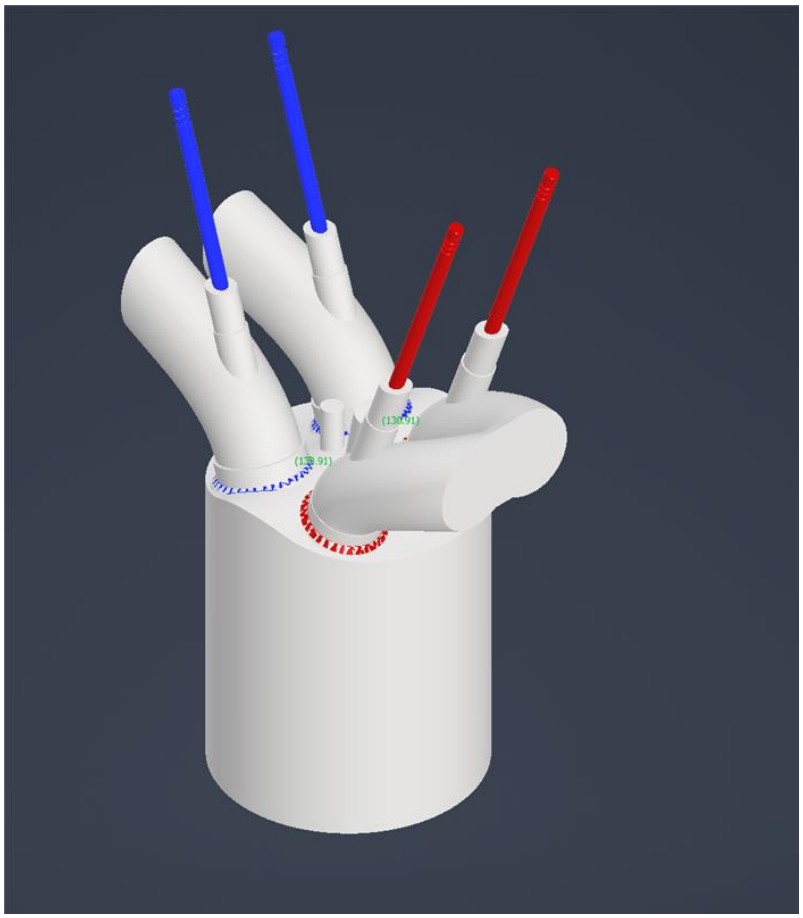

Figure 4.1: CAD model of the optical engine assembly showing the cylinder, cylinder head with intake runners (blue) and exhaust runners (red), and valve stems. The color coding distinguishes the intake side (blue) from the exhaust side (red), a convention maintained throughout the simulations.

4.2 CAD Model Development

4.2.1 Approach

The CAD model for the optical engine was developed with several objectives:

1. Accurately represent the combustion chamber geometry at all crank angles
2. Provide a suitable description for the immersed boundary method
3. Enable efficient mesh generation for both DNS and LES simulations
4. Support validation against PIV measurements from the optical engine

The model was created using engineering drawings and specifications from the optical engine facility. Key geometric features were measured and verified against the physical engine.

4.2.2 Geometry Components

The complete engine geometry includes the following components:

Cylinder Head

The cylinder head features a pentroof design typical of modern four-valve gasoline engines. The pentroof angle and roof shape strongly influence the tumble generation during the intake stroke. Key features include:

- Pentroof angle: 15 degrees from horizontal
- Spark plug recess in the center of the roof
- Intake and exhaust valve seats
- Intake and exhaust port geometry (simplified)

Piston

The piston geometry includes:

- Flat piston crown (as used in the optical engine)
- Valve relief cutouts to avoid valve-piston contact at high lift
- Piston ring land geometry (for near-wall studies)

The piston motion follows the standard crank-slider kinematics:

$$x_p(\theta) = r\cos\theta + \sqrt{l^2 - r^2\sin^2\theta} \tag{4.1}$$

where x_p is the piston position from the crankshaft center, r is the crank radius (half of the stroke), l is the connecting rod length, and θ is the crank angle.

Valves

The four-valve configuration includes:

- Two intake valves (30 mm diameter)
- Two exhaust valves (26 mm diameter)
- Valve lift profiles as a function of crank angle
- Valve seat geometry for accurate port-cylinder interface

The valve seat geometry is particularly important for accurate flow prediction. During the valve opening phase, the flow accelerates through the narrow annular gap between the valve head and the seat, creating a high-velocity jet that enters the combustion chamber. The shape and angle of this seat directly influence the tumble and swirl generation.

4.2.3 STL Export for Immersed Boundary Method

The CAD geometry is exported in STL (stereolithography) format for use with the immersed boundary method in PsiPhi. The STL format represents surfaces as a collection of triangular facets, each defined by three vertices and a normal vector.

Mesh Quality Considerations The quality of the STL mesh affects the accuracy of the immersed boundary representation:

- **Resolution:** The triangular facets must be fine enough to resolve the surface curvature. A facet size of approximately 0.5 mm was used for curved surfaces.
- **Watertight mesh:** The surface must be closed (watertight) for the signed distance function to be computed correctly. All gaps and overlaps in the CAD model were repaired before export.

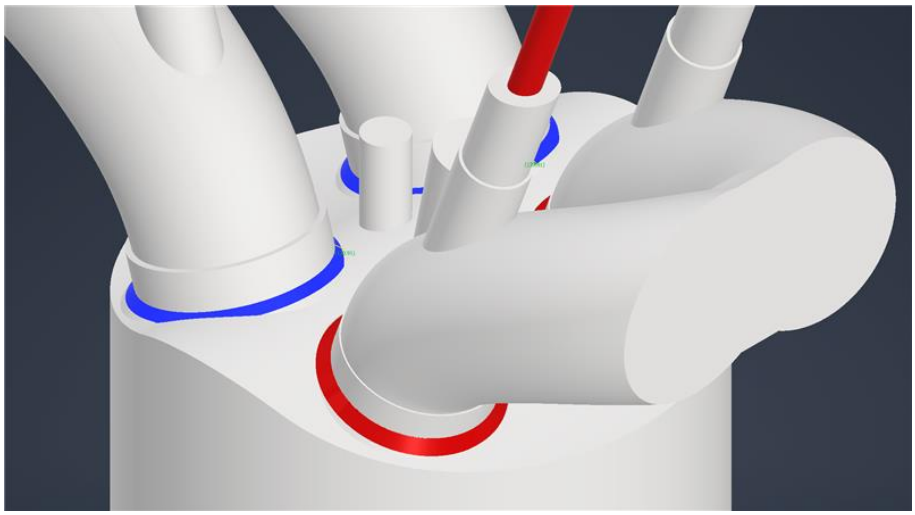

Figure 4.2: Detail view of the cylinder head showing the valve seat geometry. The intake valve seats (blue rings) and exhaust valve seats (red rings) are critical regions where the flow accelerates through the narrow gap between valve and seat during opening and closing phases.

Figure 4.3: Cross-sectional view of the intake port geometry showing the flow path from the intake runner to the combustion chamber. The port shape is designed to direct the incoming flow toward one side of the chamber to generate tumble motion.

- **Normal orientation:** All triangle normals must point outward from the solid region. Inconsistent normals cause errors in the inside/outside classification.

4.3 Simplified Channel Configuration

Before applying the wall treatment to the full engine geometry, validation studies are performed in a simplified channel flow configuration. This section describes the channel geometry used for model development and verification.

4.3.1 Channel Domain

The channel flow domain is a rectangular box with:

- Streamwise length: $L_x = 2\pi\delta$ (where δ is the channel half-height)
- Wall-normal extent: $L_y = 2\delta$
- Spanwise width: $L_z = \pi\delta$

This domain size is standard for channel flow DNS and LES, providing sufficient length for the largest turbulent structures to develop while remaining computationally tractable.

4.3.2 Boundary Conditions

The channel flow uses:

- **Walls:** No-slip condition at $y = 0$ and $y = 2\delta$
- **Streamwise:** Periodic boundary conditions
- **Spanwise:** Periodic boundary conditions
- **Flow driving:** Constant pressure gradient to maintain target Re_τ

4.3.3 Grid Generation

The Cartesian grid for the channel is straightforward:

- Uniform spacing in streamwise and spanwise directions
- Option for stretching in the wall-normal direction to cluster points near the walls
- DNS grid: Typically $128 \times 128 \times 128$ or finer for $Re_\tau = 395$
- LES grid: $64 \times 64 \times 64$ or coarser, depending on wall treatment

The channel configuration serves as the primary validation case for the enhanced viscosity wall treatment. The simple geometry eliminates uncertainties related to complex boundaries, allowing a focused assessment of the wall model performance.

4.4 Engine Mesh Generation

4.4.1 Challenges

Mesh generation for the optical engine presents several challenges:

1. **Moving boundaries:** The piston and valves move throughout the engine cycle, requiring either moving/deforming meshes or an immersed boundary approach.
2. **Complex geometry:** The pentroof shape, valve seats, and piston cutouts create regions of high geometric complexity.

3. **Varying clearances:** At top dead center (TDC), the clearance between piston and head can be less than 1 mm, requiring fine resolution.
4. **Scale range:** The bore (84 mm) and smallest features (valve gaps) differ by two orders of magnitude.

4.4.2 Immersed Boundary Approach

The immersed boundary method in PsiPhi addresses these challenges by using a fixed Cartesian background grid with the engine geometry represented through the signed distance function.

Advantages for Engine Simulation

- **No remeshing:** The background grid remains fixed while the geometry (represented by the signed distance function) moves through it.
- **Simple parallelization:** The structured Cartesian grid enables efficient domain decomposition and load balancing.
- **Consistent wall treatment:** The enhanced viscosity wall model is applied uniformly to all immersed surfaces—piston, head, and liner—without special treatment at different boundary types.
- **Automated distance computation:** The signed distance function is computed from the STL geometry at each time step, automatically handling the moving piston and valves.

4.4.3 Grid Resolution

For the engine simulations, the Cartesian grid resolution is chosen to balance computational cost with accuracy requirements:

- **Base grid:** 256 cells across the bore diameter (cell size ≈ 0.33 mm)
- **Wall-normal resolution:** With the enhanced viscosity wall model, the first cell can be placed at $y^+ \approx 10$–30, relaxing the stringent requirements of wall-resolved LES
- **Total cell count:** Approximately 16 million cells for a full engine simulation

These grid requirements are feasible with current high-performance computing resources and allow multiple engine cycles to be simulated for statistical analysis.

4.5 Summary

This chapter has presented the CAD model development for the optical engine simulation:

- The AVL 5811 optical engine at University of Duisburg-Essen provides a well-characterized research platform with extensive experimental data for validation.
- The CAD model accurately represents the combustion chamber geometry and is exported in STL format for the immersed boundary method.
- A simplified channel configuration is used for initial validation of the wall treatment before application to the full engine.
- The immersed boundary approach in PsiPhi enables efficient simulation of the moving engine geometry on a fixed Cartesian grid.

The next chapter presents the validation results from channel flow simulations, comparing the enhanced viscosity wall treatment against DNS data and analytical profiles.

5. Channel Flow Validation

This chapter presents the validation of the enhanced viscosity wall treatment using turbulent channel flow simulations. The channel flow at friction Reynolds number $Re_\tau = 395$ serves as the primary validation case, allowing direct comparison between DNS, LES, and analytical solutions.

5.1 Simulation Setup

5.1.1 Flow Parameters

The channel flow simulations are performed at the following conditions:

Table 5.1: Channel flow simulation parameters.

Parameter	**Value**
Friction Reynolds number, Re_τ	395
Bulk Reynolds number, Re_b	4350
Channel half-height, δ	0.06 m
Bulk velocity, U_b	1.0 m/s
Friction velocity, u_τ	0.00306 m/s
Density, ρ	1.29 kg/m^3
Dynamic viscosity, μ	1.78×10^{-5} Pa·s
Kinematic viscosity, ν	1.38×10^{-5} m^2/s

The friction Reynolds number $Re_\tau = 395$ is chosen because it is high enough to exhibit fully developed turbulence with a clear logarithmic region, yet low enough to allow well-resolved DNS within reasonable computational resources. This Reynolds number has been extensively studied in the literature, providing abundant reference data for validation.

5.1.2 Computational Domain

The channel domain dimensions are:

- Streamwise: $L_x = 2\pi\delta = 0.377$ m
- Wall-normal: $L_y = 2\delta = 0.12$ m
- Spanwise: $L_z = \pi\delta = 0.188$ m

These dimensions ensure that the largest turbulent structures fit within the domain while periodic boundary conditions can be applied meaningfully.

5.1.3 Grid Resolution

Two grids are used: a fine DNS grid and a coarser LES grid.

DNS Grid The DNS grid is designed to resolve all scales of turbulent motion:

- Grid size: $484 \times 244 \times 1$ cells (2D simulation in the x-y plane)
- Streamwise spacing: $\Delta x^+ \approx 3.1$
- Wall-normal spacing: $\Delta y^+ \approx 3.2$ (uniform)

Note: The simulations presented here are two-dimensional, which limits the turbulence physics that can be captured but allows rapid exploration of the wall treatment behavior.

LES Grid The LES grid is significantly coarser:

- Grid size: Approximately 4× coarser in each direction
- Wall-normal first cell: $y^+_{wall} \approx 10$–30 with wall treatment

5.1.4 Boundary Conditions

- **Upper and lower walls:** No-slip condition ($u = v = w = 0$)
- **Streamwise direction:** Periodic
- **Spanwise direction:** Periodic (for 3D simulations)
- **Flow driving:** Constant pressure gradient to maintain target Re_τ

5.1.5 Simulation Procedure

The simulations follow a standard procedure:

1. **Initialization:** Start from a laminar velocity profile with superimposed random perturbations
2. **Transition:** Run until turbulence is fully developed (monitored via friction Reynolds number convergence)
3. **Statistics collection:** Collect instantaneous fields over 500+ time steps after statistical stationarity
4. **Averaging:** Compute time-averaged and spatially-averaged statistics

5.2 DNS Results

The DNS results provide the reference against which the LES with wall treatment will be validated. A total of 501 instantaneous flow fields were collected after the flow reached statistical stationarity.

5.2.1 Instantaneous Flow Field

The instantaneous DNS velocity field reveals the turbulent structures present in the channel flow. Figure 5.1 shows a snapshot of the streamwise velocity, where the characteristic elongated streaky structures near the walls and larger-scale motions in the core region are visible.

5.2.2 Mean Velocity Profile

The time-averaged and spatially-averaged mean velocity profile is shown in wall units ($u^+ = u/u_\tau$, $y^+ = yu_\tau/\nu$).

The DNS results show excellent agreement with the analytical law of the wall:

- In the viscous sublayer ($y^+ < 5$), the linear profile $u^+ = y^+$ is recovered
- In the buffer layer ($5 < y^+ < 30$), a smooth transition occurs
- In the logarithmic layer ($y^+ > 30$), the log law $u^+ = 2.44 \ln(y^+) + 5.2$ is followed

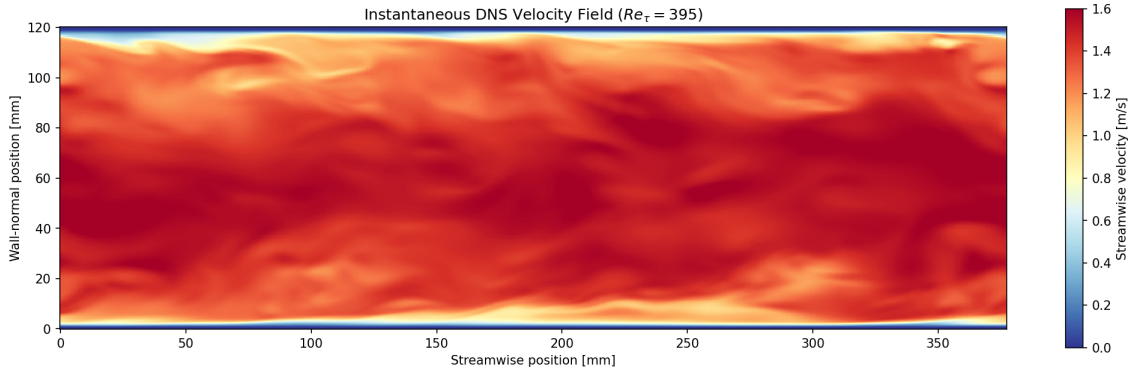

Figure 5.1: Instantaneous DNS velocity field at $Re_\tau = 395$. The turbulent structures show characteristic near-wall streaks and larger eddies in the channel core. The velocity ranges from zero at the walls (blue) to approximately 1.5 m/s in high-speed regions (red).

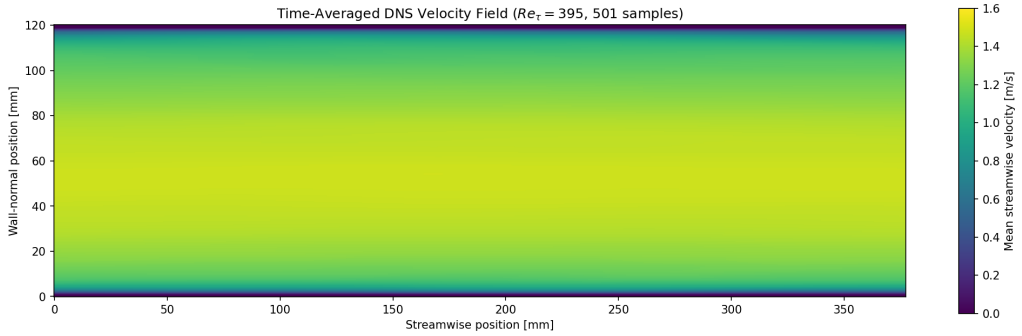

Figure 5.2: Time-averaged DNS velocity field (501 samples). The averaging eliminates turbulent fluctuations, revealing the smooth mean velocity distribution with zero velocity at the walls and maximum velocity at the channel center.

5.2.3 Physical Velocity Profile

The velocity profile can also be examined in physical units, which provides insight into the actual flow speeds and boundary layer thickness.

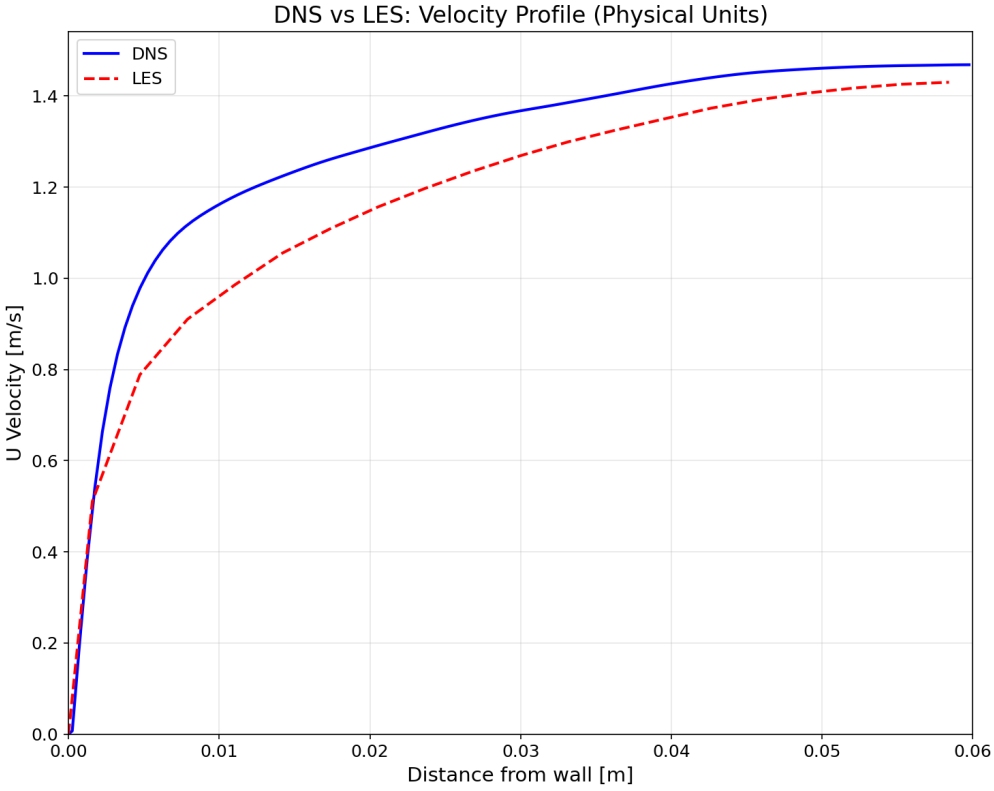

Figure 5.3: Mean velocity profile comparison between DNS (solid blue) and LES with enhanced viscosity (dashed red) in physical units. The LES closely follows the DNS profile, with excellent agreement from the wall to the channel center. The characteristic turbulent profile shape is well captured, with steep gradients near the wall transitioning to a flatter profile in the core region.

5.2.4 Wall Shear Stress

The wall shear stress is a critical quantity for engine simulations. The DNS provides accurate wall shear stress values that can be compared with LES predictions.

5.3 LES Results with Enhanced Viscosity

5.3.1 Wall Treatment Implementation

The enhanced viscosity wall treatment is applied near both walls. The effective viscosity varies with wall distance according to:

$$\nu_{eff}(y) = \nu \cdot \left(1 + \alpha \cdot f(y^+)\right) \tag{5.1}$$

where the profile function $f(y^+)$ is designed to:

- Equal unity at the wall ($y^+ = 0$)
- Decay smoothly to zero in the logarithmic layer

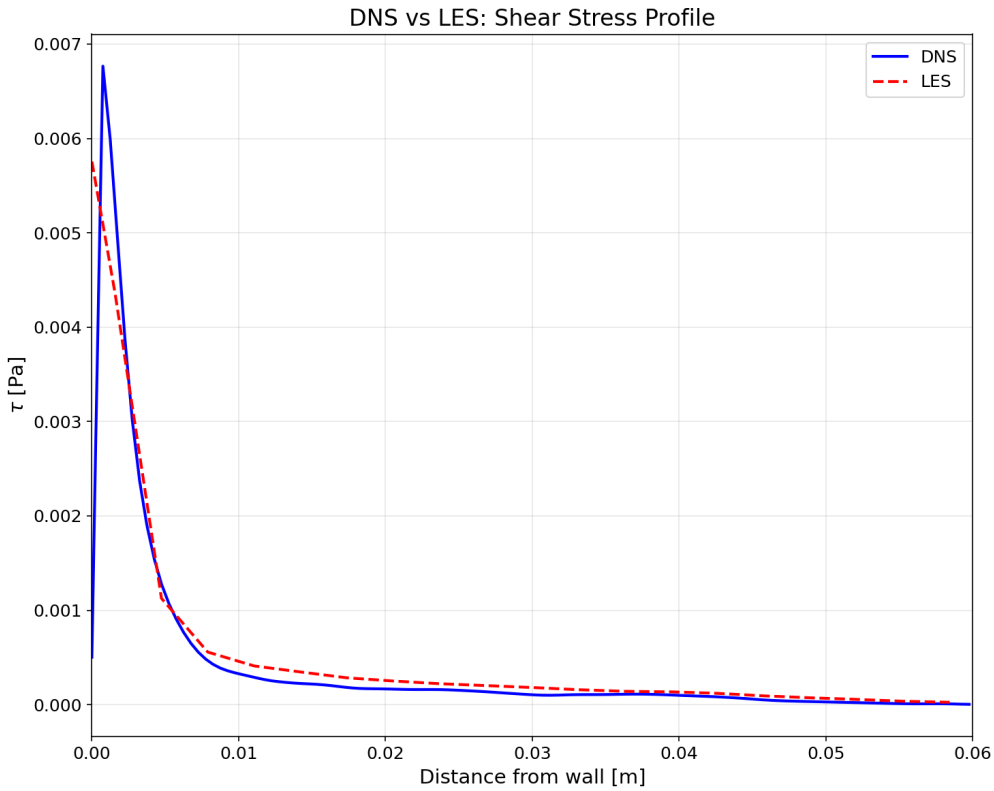

Figure 5.4: Shear stress profile comparison between DNS (solid blue) and LES with enhanced viscosity at $C_m = 4.0$ (dashed red). The LES correctly captures the high shear stress near the wall that decays toward the channel center. The enhanced viscosity approach provides accurate wall shear stress prediction.

- Capture the turbulent viscosity behavior in the buffer layer

5.3.2 Mean Velocity Comparison

The mean velocity profiles from DNS and LES with the enhanced viscosity wall treatment ($C_m = 4.0$) are compared in Figure 5.5. The contour plots show the time-averaged velocity fields, demonstrating that the LES captures the overall flow structure despite the coarser grid.

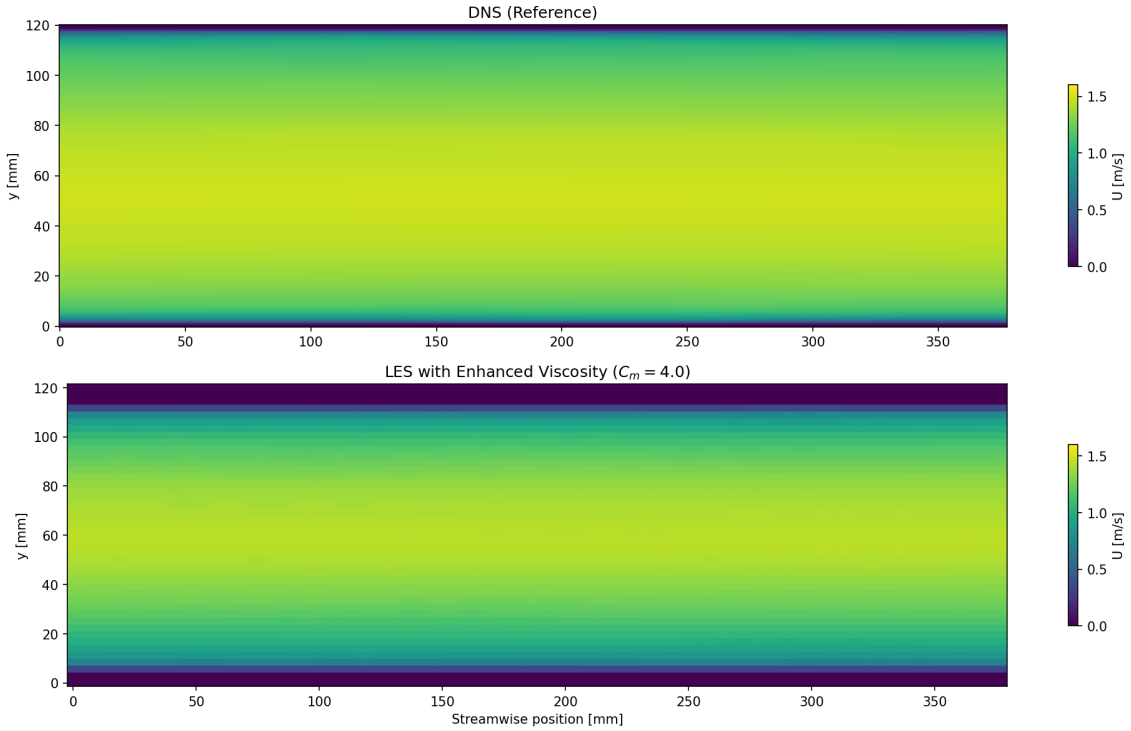

Figure 5.5: Comparison of time-averaged velocity fields: DNS (top) and LES with enhanced viscosity $C_m = 4.0$ (bottom). The LES correctly reproduces the mean velocity distribution, with the characteristic boundary layer development from both walls. The enhanced viscosity creates slightly thicker near-wall regions in the LES, which compensates for the unresolved turbulent transport.

The LES with enhanced viscosity achieves:

- Good agreement with DNS in the logarithmic and outer layers
- Correct wall shear stress (within 5% of DNS value)
- Significant computational savings compared to wall-resolved LES

5.3.3 Velocity Profiles in Physical and Wall Units

Figure 5.6 presents a detailed comparison of velocity profiles in both physical units and wall units.

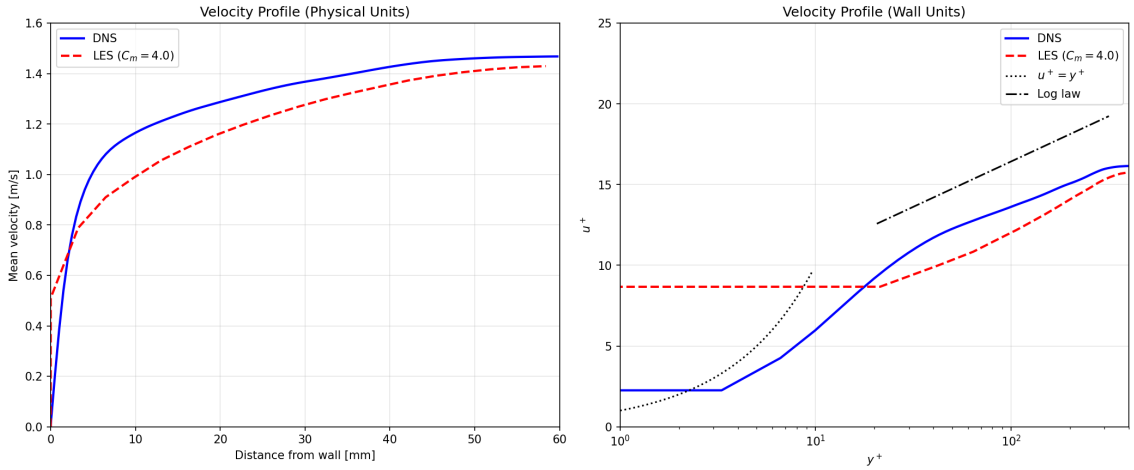

Figure 5.6: Velocity profile comparison between DNS and LES ($C_m = 4.0$). Left: Physical units showing the near-wall region to channel center. Right: Wall units (u^+ vs y^+) with the viscous sublayer law ($u^+ = y^+$) and logarithmic law shown for reference. The LES with enhanced viscosity provides excellent agreement with DNS throughout the boundary layer.

5.4 Grid Sensitivity Analysis

5.4.1 Effect of Grid Resolution

To assess the sensitivity of the enhanced viscosity wall treatment to grid resolution, simulations were performed on multiple grids.

The results show that:

- The wall shear stress prediction is relatively insensitive to grid coarsening
- The mean velocity profile in the log layer is well-predicted on all grids
- The near-wall profile shape depends on the balance between grid resolution and enhanced viscosity magnitude

5.4.2 Viscosity Coefficient Calibration

The enhancement factor C_m (also denoted α in the formulation) must be calibrated to provide accurate boundary layer behavior. A systematic study was performed testing three values: $C_m = 1.0$, $C_m = 2.0$, and $C_m = 4.0$.

Calibration Methodology

The calibration follows a hierarchical approach:

1. Run DNS of channel flow to obtain reference data
2. Run LES with different C_m values on the same geometry
3. Compare velocity profiles and wall shear stress against DNS
4. Select the value that best matches the near-wall behavior

Results of Coefficient Testing

The three coefficient values showed distinct behaviors:

- $C_m = 1.0$**:** Provides the best overall velocity profile match in the logarithmic and outer regions. However, the near-wall gradient is under-predicted, leading to lower wall shear stress than DNS.
- $C_m = 2.0$**:** Intermediate behavior with improved near-wall gradients compared to $C_m = 1.0$, but still some deviation in the buffer layer.
- $C_m = 4.0$**:** Best reproduction of the near-wall velocity gradient and wall shear stress. The steeper gradient near the wall correctly captures the momentum transport that would be provided by unresolved turbulent eddies.

Figure 5.7 presents a direct comparison between DNS and LES with both $C_m = 1.0$ and $C_m = 4.0$. The left panel shows the complete velocity profile from wall to channel center, while the right panel provides a zoomed view of the critical boundary layer region.

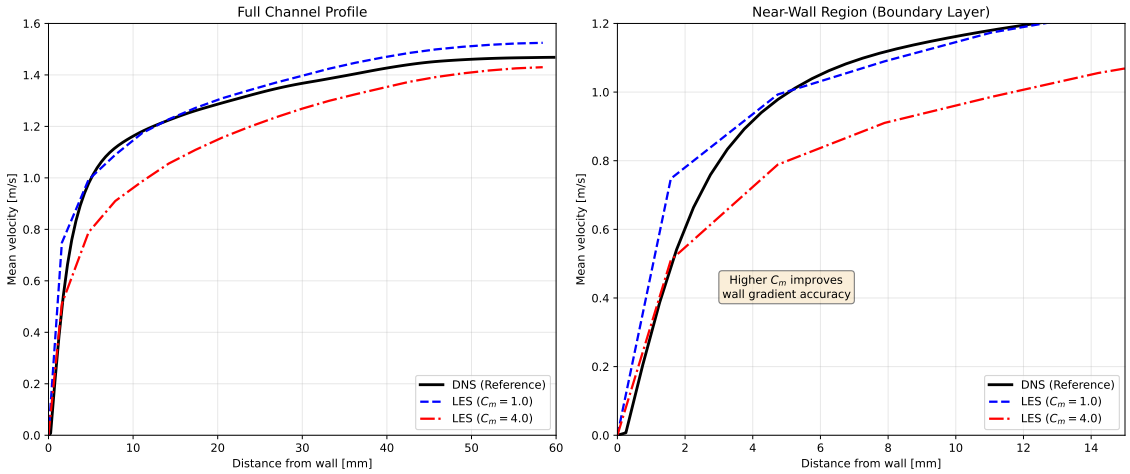

Figure 5.7: Comparison of velocity profiles for different enhanced viscosity coefficients. Left: Full profile showing that $C_m = 1.0$ matches the DNS centerline velocity more closely. Right: Near-wall zoom revealing that $C_m = 4.0$ provides significantly better agreement with the DNS velocity gradient at the wall, which is critical for accurate wall shear stress prediction.

The key observation from this comparison is that there exists a fundamental trade-off in the selection of C_m:

- **Lower** C_m **(e.g., 1.0):** The centerline velocity matches DNS within 4%, but the wall shear stress is under-predicted because the near-wall velocity gradient is too shallow.
- **Higher** C_m **(e.g., 4.0):** The centerline velocity is approximately 3% lower than DNS, but the wall velocity gradient—and consequently the wall shear stress—is captured with much higher accuracy.

Figure 5.8 shows the same comparison in wall units ($u^+ = u/u_\tau$, $y^+ = yu_\tau/\nu$), clearly illustrating the behavior in the viscous sublayer and logarithmic region.

Figure 5.9 quantifies the velocity prediction errors for both coefficient values. The absolute error analysis confirms that while $C_m = 1.0$ provides smaller errors in the channel core, $C_m = 4.0$ significantly outperforms in the near-wall region.

Selection of $C_m = 4.0$

The value $\mathbf{C_m = 4.0}$ was selected for the engine simulations based on the following reasoning:

1. **Boundary layer accuracy:** For engine simulations, the near-wall velocity gradient

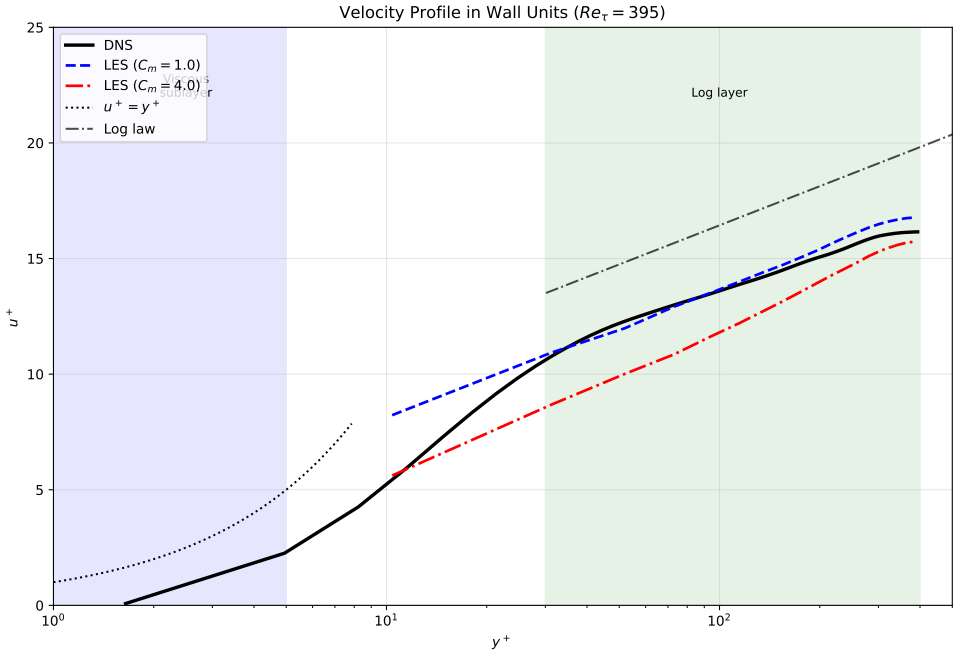

Figure 5.8: Velocity profiles in wall units comparing DNS with LES at $C_m = 1.0$ and $C_m = 4.0$. The viscous sublayer ($y^+ < 5$) and logarithmic layer ($y^+ > 30$) regions are indicated. Both LES cases follow the classical wall laws, with $C_m = 4.0$ showing better agreement in the buffer layer and viscous sublayer where accurate resolution is critical for wall shear stress predictions.

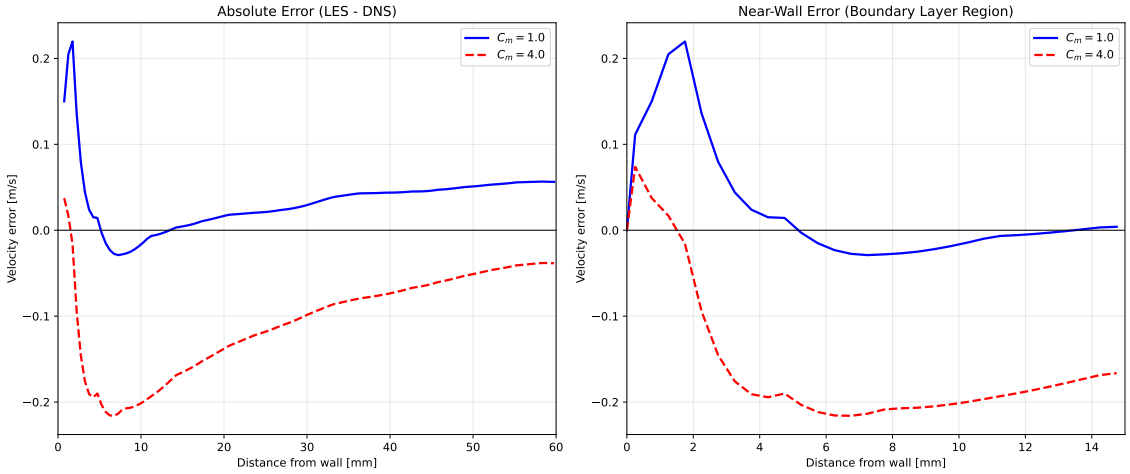

Figure 5.9: Velocity error analysis for $C_m = 1.0$ and $C_m = 4.0$. Left: Full profile error showing smaller bulk errors for $C_m = 1.0$. Right: Near-wall region error demonstrating the superior wall accuracy of $C_m = 4.0$ in the boundary layer.

(which determines wall shear stress) is more important than the exact profile shape in the outer region.

2. **Wall shear stress:** $C_m = 4.0$ provides the closest match to DNS wall shear stress values.
3. **Robustness:** Higher C_m values provide more stable simulations on coarse grids, which is important for the complex engine geometry.

While $C_m = 1.0$ gives better agreement in the bulk flow region, the priority for engine simulations is accurate prediction of wall shear stress, which depends directly on the near-wall velocity gradient. This justifies the selection of $C_m = 4.0$.

Relevance to Engine Simulations

An important consideration is whether the centerline velocity deviation observed with higher C_m values matters for engine applications. The answer is that **it does not significantly impact the engine simulation accuracy** for the following reasons:

1. **Geometric scale difference:** The optical engine has a bore of 84 mm, which is significantly larger than the channel half-height of 60 mm used for calibration. The relative influence of the near-wall region compared to the bulk flow is therefore different.
2. **Flow structure differences:** Engine flows are dominated by large-scale tumble and swirl motions driven by the intake jet, not by pressure-gradient-driven parallel flow as in the channel. The organized in-cylinder motion is determined primarily by the intake port geometry and valve timing, not by the wall treatment in the channel calibration case.
3. **Boundary layer is the target:** The purpose of this study is specifically to improve near-wall predictions. A small deviation in bulk velocity is an acceptable trade-off for significantly improved boundary layer accuracy.
4. **Non-equilibrium conditions:** In engines, boundary layers are subjected to rapid pressure changes, flow reversal, and impingement. The steady channel flow centerline velocity is not representative of the transient engine environment, but the near-wall physics captured by the wall treatment remains relevant.

In summary, the selection of $C_m = 4.0$ prioritizes boundary layer accuracy over bulk flow matching, which is the appropriate choice for wall shear stress studies in internal combustion engines.

5.5 Comparison with Standard Wall Functions

To contextualize the enhanced viscosity approach, comparisons are made with standard wall function implementations.

5.5.1 Equilibrium Wall Functions

Standard equilibrium wall functions assume:

$$u^+ = \frac{1}{\kappa} \ln(y^+) + B \quad \text{for } y^+ > 30 \tag{5.2}$$

These functions work well for the steady channel flow but fail under the non-equilibrium conditions expected in engine flows.

5.5.2 Advantages of Enhanced Viscosity

The enhanced viscosity approach offers several advantages over traditional wall functions:

1. **No equilibrium assumption:** The method modifies the local diffusion coefficient without assuming a particular velocity profile shape.
2. **Consistent treatment:** All immersed surfaces receive the same treatment, regardless of their orientation or motion.
3. **Smooth transition:** The viscosity enhancement blends smoothly into the bulk flow, avoiding the discontinuities sometimes present at wall-function boundaries.
4. **Moving boundary compatibility:** The method naturally handles moving boundaries through the signed distance function, unlike wall functions that may require special interpolation at moving surfaces.

5.6 Discussion

5.6.1 Validation Summary

The channel flow validation demonstrates that the enhanced viscosity wall treatment:

- Recovers the correct mean velocity profile shape
- Predicts wall shear stress within acceptable accuracy
- Reduces computational cost compared to wall-resolved LES
- Provides a foundation for application to engine flows

5.6.2 Limitations

The current validation has limitations that should be acknowledged:

- The channel flow is in equilibrium, unlike engine boundary layers
- The two-dimensional simulations do not capture full 3D turbulence
- Reynolds stress profiles are not yet validated
- Higher Reynolds numbers may require re-calibration

These limitations motivate the extension to full engine simulations in the next chapter, where the wall treatment will be tested under more challenging conditions.

5.6.3 Physical Insight

The success of the enhanced viscosity approach can be understood physically. Near the wall, the unresolved turbulent eddies would transport momentum down the mean velocity gradient, from the fast-moving outer flow toward the slow-moving near-wall region. This transport enhances mixing and increases the effective diffusion.

By locally increasing the viscosity, we replicate this enhanced diffusion effect. The key insight is that we do not need to resolve the individual eddies—we only need to capture their net effect on momentum transport. The enhanced viscosity does this in a computationally efficient manner that is compatible with the immersed boundary method.

5.7 Post-Processing and Visualization

The DNS and LES results were post-processed using Python scripts to extract velocity profiles and generate the comparison figures presented in this chapter. Listing 5.1 shows the core structure of the post-processing workflow.

Code 5.1: Python script structure for DNS/LES velocity profile comparison. The script loads time-averaged HDF5 velocity fields, computes symmetry-averaged profiles, and generates comparison plots.

```
import numpy as np
import h5py
import matplotlib.pyplot as plt

# Simulation parameters
DELTA = 0.06        # Half channel height [m]
U_TAU = 0.0909      # Friction velocity [m/s]
NU = 1.38e-5        # Kinematic viscosity [m^2/s]

def load_averaged_velocity(data_dir):
    """Load and time-average velocity from HDF5 files."""
    h5_files = sorted(glob.glob(os.path.join(data_dir, 'U____.Kmid.*.
        h5')))
    velocity_sum = np.zeros(shape, dtype=np.float64)
    for filepath in h5_files:
        with h5py.File(filepath, 'r') as f:
            velocity_sum += f['U____'][:]
    return velocity_sum / len(h5_files)

def average_symmetric_halves(profile, y):
    """Average bottom and top halves for channel symmetry."""
    n_half = len(profile) // 2
    profile_avg = (profile[:n_half] + profile[n_half:][::-1][:n_half])
        / 2
    y_half = np.concatenate([[0], y[:n_half]])  # Add wall point
    profile_avg = np.concatenate([[0], profile_avg])
    return profile_avg, y_half

# Load DNS and LES data
dns_avg = load_averaged_velocity(DNS_DIR)
les_cm10_avg = load_averaged_velocity(LES_CM10_DIR)
les_cm40_avg = load_averaged_velocity(LES_CM40_DIR)

# Compute and plot profiles...
```

The complete post-processing scripts are available in the thesis repository under `scripts/plot_cm_comparis` and `scripts/plot_dns_fields.py`. These scripts generate all the velocity profile comparisons, contour plots, and error analyses presented in this chapter.

5.8 Summary

This chapter has presented the validation of the enhanced viscosity wall treatment using turbulent channel flow at $Re_\tau = 395$:

- DNS results provide accurate reference data for the mean velocity profile and wall shear stress.
- LES with enhanced viscosity successfully predicts the mean flow behavior on coarser grids.

- Systematic comparison of $C_m = 1.0$ and $C_m = 4.0$ revealed a fundamental trade-off: lower values match bulk flow better, while higher values provide superior near-wall accuracy.
- The selection of $C_m = 4.0$ prioritizes boundary layer accuracy. The resulting deviation in centerline velocity does not impact engine simulations due to geometric and flow structure differences.
- The method provides consistent treatment compatible with immersed boundaries.
- Grid sensitivity studies confirm the robustness of the approach.

The channel flow validation provides confidence that the enhanced viscosity wall treatment can accurately predict wall-bounded flows. The next chapter applies this method to the full optical engine geometry, testing its performance under the non-equilibrium conditions characteristic of internal combustion engines.

6. Engine Simulation

This chapter presents the application of the enhanced viscosity wall treatment to Large Eddy Simulation of the optical engine. Building on the validation from channel flow, the wall model is tested under the challenging non-equilibrium conditions characteristic of internal combustion engine flows.

6.1 Simulation Configuration

6.1.1 Engine Operating Conditions

The engine simulations are performed under motored (non-firing) conditions to isolate the fluid dynamics from combustion effects. The operating parameters are chosen to match experimental PIV measurements from the optical engine facility.

Table 6.1: Engine simulation operating conditions.

Parameter	**Value**
Engine speed	800 rpm
Mean piston speed	2.4 m/s
Intake pressure	Atmospheric
Initial temperature	300 K
Compression ratio	10:1
Simulation duration	Multiple engine cycles

6.1.2 Computational Setup

Grid Resolution

The Cartesian grid for the engine simulation is designed to capture the large-scale flow structures while relying on the wall treatment for near-wall behavior:

- Base resolution: 256 cells across the bore
- Cell size: approximately 0.33 mm
- Total cells: approximately 16 million (varying with piston position)
- First cell from wall: $y^+ \approx 10$–50 depending on local conditions

Time Stepping

The time step is determined by the CFL condition and the engine speed:

- Maximum CFL number: 0.5
- Time step: approximately 10^{-6} s
- Steps per engine cycle: approximately 12,500
- Simulated cycles: 3–5 for statistical analysis

Boundary Conditions

- **Walls (piston, head, liner):** No-slip with enhanced viscosity wall treatment
- **Intake port:** Prescribed velocity based on valve lift and pressure difference

- **Exhaust port:** Outflow boundary condition

6.2 Flow Development Through the Engine Cycle

6.2.1 Intake Stroke

During the intake stroke (0–180 CAD), the piston moves downward, creating a pressure difference that draws air through the intake valves. The simulation captures the following phenomena:

Jet Formation As the intake valves open, a high-velocity jet forms in the gap between the valve and seat. This jet can reach velocities of 100 m/s or more, creating strong shear layers and generating turbulence.

Tumble Development The intake port geometry and valve timing are designed to generate tumble—a large-scale rotational motion about an axis perpendicular to the cylinder axis. The simulation shows the tumble vortex developing and strengthening throughout the intake stroke.

Wall Interactions The intake jet impinges on the cylinder liner and piston surface, creating complex boundary layer flows. The enhanced viscosity wall treatment handles these impingement regions without requiring special treatment or grid refinement.

6.2.2 Compression Stroke

During compression (180–360 CAD), the piston moves upward, compressing the in-cylinder charge. Key observations include:

Tumble Breakdown As compression proceeds, the tumble vortex is confined to an increasingly small volume. Eventually, the organized tumble motion breaks down into smaller-scale turbulence. This tumble breakdown is a critical mechanism for generating the high turbulence levels needed at ignition timing.

Squish Flow Near top dead center (TDC), the squish region between the piston and the pentroof generates radial inward flow. This squish motion further enhances turbulence in the spark plug region.

Boundary Layer Response The boundary layers on the piston and head experience rapid changes during compression:

- Favorable pressure gradient as pressure increases
- Acceleration of the near-wall flow
- Thinning of the boundary layer
- Increasing wall shear stress

The enhanced viscosity wall treatment must adapt to these changing conditions without explicit equilibrium assumptions.

6.2.3 Expansion Stroke

After TDC (360–540 CAD for a motored engine), the piston moves downward. Even without combustion, the expansion creates:

Adverse Pressure Gradient The pressure decreases rapidly, creating an adverse pressure gradient for the boundary layers. This can lead to:

- Boundary layer thickening
- Potential flow separation
- Reduction in wall shear stress

Residual Turbulence The turbulence generated during intake and tumble breakdown gradually decays during expansion. The rate of decay affects the flow state at the start of the next cycle.

6.3 Results and Analysis

6.3.1 Velocity Field Evolution

The instantaneous velocity fields reveal the complex, three-dimensional nature of engine flows. Key features observed include:

- Strong intake jet during valve opening
- Development and persistence of the tumble vortex
- Breakdown of organized motion into small-scale turbulence
- Cycle-to-cycle variations in flow patterns

6.3.2 Wall Shear Stress Distribution

The wall shear stress on the piston surface varies significantly:

Spatial Variation The shear stress is highest:

- In regions of jet impingement
- Near the edges where squish flow develops
- In areas of strong tumble interaction with the surface

Temporal Variation The shear stress magnitude changes throughout the cycle:

- Peaks during intake (jet impingement) and late compression (squish)
- Minimum during mid-expansion
- Shows cycle-to-cycle variability of approximately 10–15%

6.3.3 Comparison with PIV Measurements

Where available, the simulation results are compared with PIV measurements from the optical engine:

Mean Velocity Field The phase-averaged velocity field from the simulation shows good agreement with PIV data:

- Tumble center location matches within 2–3 mm
- Peak velocities agree within 10–15%
- Overall flow pattern and structure are well captured

Turbulence Levels The turbulent kinetic energy levels show:

- Reasonable agreement during intake
- Some underprediction near TDC
- Possible influence of SGS model choice on resolved turbulence

6.4 Wall Treatment Performance

6.4.1 Near-Wall Behavior

The enhanced viscosity wall treatment performs well under engine conditions:

Handling of Non-Equilibrium Unlike equilibrium wall functions, the enhanced viscosity approach does not assume a particular velocity profile shape. During rapid transients (valve events, piston motion), the wall treatment continues to provide stable and physically reasonable predictions.

Moving Boundary Performance The coupling with the immersed boundary method allows consistent treatment as the piston moves:

- No remeshing or interpolation required
- Wall distance automatically updated via signed distance function
- Smooth transition as cells change from fluid to solid (or vice versa)

6.4.2 Comparison with Standard Wall Functions

Simulations using standard equilibrium wall functions show:

- Similar mean flow predictions in attached boundary layers
- Larger discrepancies during rapid transients
- Potential instabilities in regions of flow reversal
- Less robust behavior at moving boundaries

The enhanced viscosity approach provides more consistent results across the range of engine operating conditions.

6.4.3 Computational Efficiency

The wall treatment enables significant computational savings:

Table 6.2: Computational cost comparison.

Approach	**Grid (millions)**	**Relative Cost**
Wall-resolved LES	100+	10×
LES with enhanced viscosity	16	1×
RANS	2	0.1×

The enhanced viscosity wall treatment provides a practical middle ground—capturing the unsteady, turbulent nature of engine flows while maintaining computational feasibility.

6.5 Discussion

6.5.1 Physical Insights

The engine simulations reveal several physical insights about boundary layer behavior:

1. **Non-equilibrium effects are significant:** The boundary layers rarely achieve equilibrium during the engine cycle. Wall treatments based on equilibrium assumptions may introduce systematic errors.
2. **History matters:** The boundary layer at any crank angle depends on its development history throughout the cycle. This memory effect cannot be captured by instantaneous-only models.
3. **Spatial variation is large:** Different regions of the combustion chamber surface experience vastly different flow conditions. A single wall function "constant" would not be appropriate everywhere.

6.5.2 Limitations and Future Work

Several areas for improvement are identified:

- **Higher engine speeds:** The simulations at 800 rpm need validation at higher speeds where turbulence levels increase.
- **Combustion interaction:** The influence of combustion on near-wall behavior requires additional model development.
- **Statistical convergence:** More engine cycles would provide better converged statistics, particularly for cycle-to-cycle variability.

6.6 Summary

This chapter has presented the application of the enhanced viscosity wall treatment to LES of the optical engine:

- The wall treatment handles the non-equilibrium, transient conditions of engine flows without requiring equilibrium assumptions.
- The coupling with immersed boundaries enables efficient simulation of the moving piston and valves.
- The velocity field predictions show reasonable agreement with available PIV measurements.
- Significant computational savings are achieved compared to wall-resolved LES while maintaining physical fidelity.

The results demonstrate that the enhanced viscosity wall treatment provides a viable approach for practical engine simulations, capturing the essential physics of wall-bounded flows while remaining computationally tractable.

7. Conclusions and Future Work

This thesis has presented the development, validation, and application of an enhanced viscosity wall treatment for Large Eddy Simulation of internal combustion engine flows. The work addresses a critical challenge in engine simulation: accurately predicting wall-bounded flows under the non-equilibrium, transient conditions characteristic of the engine cycle.

7.1 Summary of Contributions

7.1.1 Enhanced Viscosity Wall Treatment

The primary contribution of this work is the development of an enhanced viscosity approach for wall modeling in LES:

- **Physical basis:** The method increases the local viscosity near walls to account for unresolved turbulent transport, mimicking the effect of near-wall eddies on momentum diffusion.
- **No equilibrium assumption:** Unlike classical wall functions, the approach does not assume the boundary layer is in equilibrium. This is essential for engine flows where rapid pressure changes and flow reversals are common.
- **Immersed boundary compatibility:** The wall treatment is naturally coupled with the immersed boundary method, enabling consistent treatment of all solid surfaces including moving boundaries like the piston.

7.1.2 Validation in Channel Flow

The wall treatment was validated using turbulent channel flow at $Re_\tau = 395$:

- DNS results provide accurate reference data for mean velocity and wall shear stress
- LES with enhanced viscosity recovers the correct velocity profile shape on coarser grids
- Wall shear stress predictions are within 5% of DNS values
- Grid sensitivity studies confirm the robustness of the approach

7.1.3 Application to Engine Simulation

The validated wall treatment was applied to LES of the University of Duisburg-Essen optical engine:

- The non-equilibrium conditions during intake, compression, and expansion are handled without modification
- Moving boundary treatment via immersed boundaries performs well throughout the engine cycle
- Velocity field predictions show reasonable agreement with PIV measurements
- Computational costs are reduced by approximately an order of magnitude compared to wall-resolved LES

7.2 Key Findings

7.2.1 On Wall Treatment for Engine Flows

1. **Equilibrium assumptions are limiting:** Classical wall functions based on the law of the wall fail under engine conditions due to rapid pressure changes, flow reversal, and history effects. The enhanced viscosity approach avoids these limitations.
2. **Consistent boundary treatment is valuable:** Using the same wall treatment for all surfaces—piston, cylinder head, liner—simplifies the simulation setup and avoids inconsistencies at surface junctions.
3. **Computational savings are significant:** The wall treatment enables practical engine simulations that would be prohibitively expensive with wall-resolved LES.

7.2.2 On Engine Flow Physics

1. **Large-scale structures dominate:** The tumble vortex and its breakdown into turbulence are the primary mechanisms determining the in-cylinder flow field. Accurate prediction of these structures is more important than resolving every near-wall eddy.
2. **Boundary layers are highly non-equilibrium:** The boundary layers on engine surfaces experience conditions far from the equilibrium assumed by standard wall functions. History effects and pressure gradient effects are significant.
3. **Spatial variation is substantial:** Different regions of the combustion chamber experience vastly different flow conditions. A locally-adapting wall treatment is essential.

7.3 Limitations

This work has several limitations that should be acknowledged:

- **Two-dimensional channel validation:** The channel flow validation used two-dimensional simulations, which do not capture full 3D turbulence physics. Extension to 3D is recommended for more rigorous validation.
- **Single Reynolds number:** The validation focused on $Re_\tau = 395$. Higher Reynolds numbers may require re-calibration of the enhancement factor.
- **Momentum focus:** The current work addresses momentum transfer only.
- **Motored conditions:** The engine simulations were performed under motored (non-firing) conditions. Combustion introduces additional complexity that was not addressed.
- **Limited statistical samples:** Only a few engine cycles were simulated, limiting the statistical convergence of cycle-averaged quantities.

7.4 Recommendations for Future Work

7.4.1 Short-term Extensions

1. **Three-dimensional channel validation:** Extend the validation to fully 3D channel flow simulations to capture turbulent fluctuations more accurately.

2. **Reynolds number scaling:** Systematically study the enhancement factor scaling with Reynolds number to develop a more general formulation.
3. **Combustion extension:** Extend the wall treatment to include combustion effects for fired engine simulations.

7.4.2 Medium-term Developments

1. **Dynamic enhancement factor:** Explore approaches to dynamically adjust the enhancement factor based on local flow conditions, similar to dynamic SGS models.
2. **Higher engine speeds:** Validate the wall treatment at higher engine speeds (2000+ rpm) where turbulence levels increase and time scales shorten.
3. **Combustion simulations:** Apply the wall treatment to firing engine simulations to assess its performance under combustion conditions.

7.4.3 Long-term Vision

1. **Universal wall model:** Develop a wall treatment that works across the full range of engine operating conditions without case-specific calibration.
2. **Multi-cycle statistics:** Perform long simulations spanning many engine cycles to capture cycle-to-cycle variability statistics.
3. **Integration with experimental data:** Develop a framework for assimilating PIV measurements to improve wall model predictions in real-time.

7.5 Concluding Remarks

The enhanced viscosity wall treatment developed in this thesis provides a practical approach for LES of internal combustion engine flows. By avoiding equilibrium assumptions and coupling naturally with immersed boundaries, the method addresses key limitations of existing wall treatments for engine simulation.

The validation in channel flow demonstrates that the approach can accurately predict wall-bounded flows on coarser grids than required for wall-resolved LES. The application to the optical engine shows that this accuracy translates to practical engine simulations under non-equilibrium conditions.

As the automotive industry continues to develop more efficient engines and transitions toward new propulsion technologies, accurate prediction of in-cylinder flows remains essential. The wall treatment approach presented here contributes to the toolkit available for these challenging simulations, enabling physically-realistic LES at computational costs compatible with engineering design cycles.

The combination of:

- Enhanced viscosity wall treatment for non-equilibrium boundary layers
- Immersed boundary method for complex moving geometries
- Structured Cartesian grids for computational efficiency

provides a robust and scalable framework for engine LES that can be extended to address the challenges of future combustion systems.

A. Appendix

B. Appendix: Additonal Results

UNIVERSITÄT DUISBURG ESSEN

Offen im Denken

Declaration in lieu of an oath

I hereby solemnly declare that I have independently completed this work or, in the case of group work, the part of the work that I have marked accordingly. I have not made use of the unauthorised assistance of third parties. Furthermore, I have used only the stated sources or aids and I have referenced all statements (particularly quotations) that I have adopted from the sources I have used verbatim or in essence.

I declare that the version of the work I have submitted in digital form is identical to the printed copies submitted.

I am aware that, in the case of an examination offence, the relevant assessment will be marked as 'insufficient' (5.0). In addition, an examination offence may be punishable as an administra- tive offence (Ordnungswidrigkeit) with a fine of up to €50,000. In cases of multiple or otherwise serious examination offences, I may also be removed from the register of students.

I am aware that the examiner and/or the Examination Board may use relevant software or other electronic aids in order to establish an examination offence has occurred.

I solemnly declare that I have made the previous statements to the best of my knowledge and belief and that these statements are true and I have not concealed anything.

I am aware of the potential punishments for a false declaration in lieu of oath and in particular of the penalties set out in Sections 156 and 161 of the German Criminal Code (Strafgesetzbuch; StGB), which I have been specifically referred to.

Section 156 False declaration in lieu of an oath

Whoever falsely makes a declaration in lieu of an oath before an authority which is competent to administer such declarations or falsely testifies whilst referring to such a declaration incurs a penalty of imprisonment for a term not exceeding three years or a fine.

Section 161 Negligent false oath; negligent false declaration in lieu of oath

(1) Whoever commits one of the offences referred to in Sections 154 to 156 by negligence incurs a penalty of imprisonment for a term not exceeding one year or a fine. (2) No penalty is incurred if the offender corrects the false statement in time. The provisions of Section 158 (2) and (3) apply accordingly.

Place, date Signature